Chemosphere 263 (2021) 128244

Contents lists available at ScienceDirect

Chemosphere

journal homepage: www.elsevier.com/locate/chemosphere

Photocatalytic remediation of organic waste over Keggin-based polyoxometalate materials: A review

Sin Yuan Lai [a, c, *], Kim Hoong Ng [b, c, **], Chin Kui Cheng [d], Hadi Nur [e, f], Mukhamad Nurhadi [g], Mahashanon Arumugam [a, c, h]

[a] School of Energy and Chemical Engineering, Xiamen University Malaysia, Selangor Darul Ehsan, 43900, Malaysia
[b] College of Chemical Engineering, Fuzhou University, Fuzhou, 350116, PR China
[c] College of Chemistry and Chemical Engineering, Xiamen University, Xiamen, 361005, China
[d] Department of Chemical Engineering, College of Engineering, Khalifa University, P. O. Box 127788, Abu Dhabi, United Arab Emirates
[e] Centre for Sustainable Nanomaterials, Ibnu Sina Institute for Scientific and Industrial Research, Universiti Teknologi Malaysia, UTM, Skudai, Johor, 81310, Malaysia
[f] Central Laboratory of Minerals and Advanced Materials, Faculty of Mathematics and Natural Science, Universitas Negeri Malang, Malang, 65145, Indonesia
[g] Department of Chemical Education, Universitas Mulawarman, Kampus Gunung Kelua, Samarinda, 75119, East Kalimantan, Indonesia
[h] Department of Petroleum Technology and Alternative Fuels, Faculty of Environmental Technology, UCT, Prague, Technická 5, 160 00, Praha 6-Dejvice, Czechia

HIGHLIGHTS

- Keggin-based POMs in photocatalysis was systematically introduced.
- Effects of different preparation methods were discussed.
- Practicality enhancement and process intensification were addressed.
- Photochemistry and mechanisms of binary and ternary POMs were recapitulated.
- Overview of POMs were summarized and future prospects of POMs were outlined.

ARTICLE INFO

Article history:
Received 5 July 2020
Received in revised form
17 August 2020
Accepted 2 September 2020
Available online 6 September 2020

Handling Editor: Derek Muir

Keywords:
Keggin-based polyoxometalates
Strategized preparation methods
Hierarchical enhancement
Photochemistry
Organic waste remediation

ABSTRACT

Photocatalytic remediation of industrial water pollution has courted intense attention lately due to its touted green approach. In this respect, Keggin-based polyoxometalates (POMs) as green solid acids in photocatalytic reaction possess superior qualities, *viz.* unique photoinduced charge-transfer properties, strong photooxidative-photoreductive ability, high chemical and thermal stability, and so forth. Unfortunately, it suffers from a large bandgap energy, low specific surface area, low recoverability, and scarce utilization in narrow absorption range. Therefore, the pollutant degradation performance is not satisfactory. Consequently, multifarious research to enhance the photocatalytic performance of Keggin-based POMs were reported, *viz.* via novel modifications and functionalizations through a variety of materials, inclusive of, *inter alia*, metal oxides, transition metals, noble metals, and others. In order to advocate this emerging technology, current review work provides a systematic overview on recent advancement, initiated from the strategized synthetic methods, followed by hierarchical enhancement and intensification process, at the same time emphasizes on the fundamental working principles of Keggin-based POM nanocomposites. By reviewing and summarizing the efforts adopted global-wide, this review is ended with providing useful outlooks for future studies. It is also anticipated to shed light on producing Keggin-based POM nanocomposites with breakthrough visible- and solar-light-driven photocatalytic performance against recalcitrant organic waste.

* Corresponding author. Xiamen University Malaysia, Jalan Sunsuria, Bandar Sunsuria, 43900, Sepang, Selangor, Malaysia.
** Corresponding author. College of Chemical Engineering, Fuzhou University, Fuzhou, 350116, PR China.
E-mail addresses: sinyuan.lai@xmu.edu.my (S.Y. Lai), Ng_KH1990@hotmail.com (K.H. Ng).

https://doi.org/10.1016/j.chemosphere.2020.128244
0045-6535/

Contents

1. Introduction

Organic pollutant is generally recalcitrant, and it degrades the environment substantially, particularly to water bodies. Indeed, a large number of polluting organic compounds such as methanol, aniline, *p*-nitroaniline and *o*-chlorophenol, are intractable, exhibiting mutagenic and oncogenic effects. Their biodegradation or removal process becomes extremely challenging, as these organic pollutants are highly soluble and stable within the water bodies. Moreover, organic pollutants in water systems are bioaccumulative, non-biodegradable, and highly harmful to living lives (Sagban, 2014; Xu et al., 2016). Various remediation methods, such as membrane filtration (Hir et al., 2017), adsorption (Björklund & Y.Li, 2017), biological treatment (Chowdhary et al., 2017), photocatalyts (Wu et al., 2013; Xu et al., 2016; Yahya et al., 2019), have been employed. Among the plethora of water treatments, photocatalytic degradation has been widely utilized to maintain the high quality of water and prolong the eco-friendly environment by controlling the concentration of wastewater, without causing secondary pollution (Lu et al., 2012, 2017; Rohani et al., 2017; Salavati et al., 2018; Shi et al., 2012; Yahya et al., 2019; Yan et al., 2017).

Essentially, an effective and versatile photocatalyst, commonly a semiconductor material, is used for organic pollutants degradation. There are various highly promising metal oxides (also semiconductors) examined as photocatalytic candidates. Recently, a cluster of metal oxide anions, *i.e.* polyoxometalates (abbreviated POMs), have been identified as suitable photocatalysts. Polyoxometalate is a polyatomic anion or heteropolyanion, comprised of oxygen atoms shared or linked together by early transition metals (usually Group V or VI) at their highest oxidation states and traces amount of heteroatoms (P, As, Si or Ge) (Ammam, 2013; Nikoonahad et al., 2018; Suzuki et al., 2018). It is a conjugate anion to heteropolyacid (abbreviated HPAs), forming a heteropolyacid upon associated with a hydrogen ion (H^+). Literally, heteropolyacid is a combination of 'hetero-', 'poly-' and 'acid', which explicitly described its molecular structure. For instance, "hetero" signifies trace element (P, Si, As or Ge), which is different from addenda metal oxide anions; "poly" denotes more than one addenda transition metals (W or Mo) linked by oxygen atoms; "acid" represents acidic hydrogen atoms. Succinctly, heteropolyacid is that hydrogen atoms coupled with a cluster of addenda transition metals linked by oxygen atoms with heteroatom inside it.

POMs are designed and configured into a few common structures, such as Keggin ion, Dawson ion, Preyssler ion, Anderson ion, *etc*. These POMs' design could have two anion structures of (i) fully occupied and (ii) lacunary (Fig. 1). POMs are basically formed by condensation of many addenda transition metal oxides (MO_x, M = addenda transition metals) surrounding a central heteroatom in acidic solution and then presented, in generally, as a cluster of poly(metal oxides). By further exploring the coordination of POMs, several types of chelation or linkage can be observed. Keggin and Well-Dawson structures display tetrahedral or 4-coordination (PO_4^{3-}, SiO_4^{4-}, AsO_4^{3-}), Anderson structure exhibits octahedral or 6-coordination ($Al(OH)_6^{3-}$, TeO_6^{6-}), and so forth (Omwoma et al., 2014). Unlike most of the metal oxides, POM-based nanocomposites typically contain of tens to hundreds of metal atoms, with nuclearities reaching up to 368 metal atoms in a single cluster of nanoparticles (Ammam, 2013; Nikoonahad et al., 2018; Suzuki et al., 2018). Its structure is characterized by the ratio of the heteroatoms to metal (X/M, where X = P^{5+} or Si^{4+}; M = W^{6+} or Mo^{6+}), instead of oxygen, which possesses high tunability based on the desired properties and applications. This endows the POMs with excellent versatility and accessibility to various applications in the field of electrochemistry (Ammam, 2013; Dianat et al., 2019; Liu et al., 2011; Tang et al., 2000), drug delivery (Gao et al., 2016; Karimian et al., 2017; Li et al., 2014), biosensors (Boussema et al., 2018; Mercier et al., 2015; Wang et al., 2012;Zhou et al., 2013) and catalysis (Heravi et al., 2013; Hill, 2007; Li et al., 2017; Lv et al., 2012; Mizuno et al., 2005; Taghizadeh et al., 2019; Wang and Yang, 2015). In addition, POMs also attracted considerable attention as photocatalysts (Bamoharram et al., 2013; Huang et al., 2017; Kazemi, 2017; S. Kazemi et al., 2017; Lu et al., 2017; Lu et al., 2012; Nikoonahad et al., 2018; Rohani et al., 2017; Taghavi et al., 2018; Yoon et al., 2001), bestowed to their unique photoinduced charge-

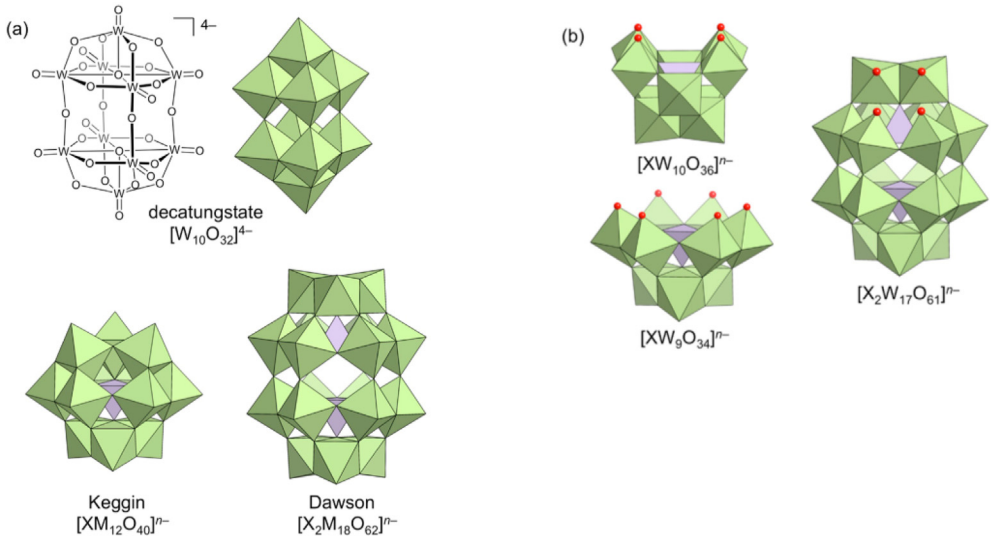

Fig. 1. Anion structures of (a) fully occupied and (b) lacunary POMs. The light-green and gray polyhedra represent 4-coordinated, $[MO_6]$ and 6-coordinated $[XO_4]$ metal oxides, respectively. The red spheres represent oxygen atoms at the vacant sites of lacunary POM. Reprinted with permission from (Suzuki et al., 2018). Copyright 2018 American Chemical Society. (For interpretation of the references to colour in this figure legend, the reader is referred to the Web version of this article.)

transfer properties, the oxidation of O_2^--based HOMOs and the reduction of Group 5 or 6-based LUMOs properties, and reactivity (Ammam, 2013; Suzuki et al., 2018).

Keggin-based POM nanocomposites has emerged to be green and eco-friendly catalysts that expanded abruptly in various applications. The photocatalyst is easily dissolve and dispersed homogeneously in water solution, enhancing its ability to dope or functionalize with other compounds. Moreover, the photocatalytic reactions are well carried out under mild conditions, such as under flow of oxygen, atmospheric pressure and room temperature. Its blooming could be also attributed to their chemical stability, versatility in composition and physical-chemical features (Kazemi, 2017). It is touted for its high chemical and mechanical resistance under reaction conditions due to its strong covalent dative bond of oxygen atoms towards metal ions (Holclajtner-Antunović et al., 2019; Oliveira et al., 2019; Salavati et al., 2018). Besides, the lowest vacant *d* molecular orbital in octahedral (MO_6) of this structure is a non-bonding metal-centered which accounted for the reversible reduction to form multivalence species (Keita et al., 2006; Wang et al., 2019; Yang et al., 2009). In addition, it also acts as a good electron acceptor for efficient electron storing (Chen et al., 2019; Gu & Shannon, 2007; Maguerès et al., 2000) that facilitates the photo-generated charges separation in photocatalysis. Therefore, it has been extensively explored as photocatalyst in recent years, arises as one of the most popular research areas in inorganic chemistry.

Although it is bestowed with a number of superiorities, application of pristine POM-based photocatalysts is still hindered from issues such as large bandgap energy (UV light responsive), low specific surface area, tend to dissociate with pH, which leading to low recoverability and low effectiveness in visible or solar light region. Therefore, modification to the existing POM structure is paramount to its wider applications. For example, the limitations of the POM nanocomposites, mainly Keggin-structured POM-based photocatalysts, could be overcome by amalgamating metal oxides (Gu and Shannon, 2007; Li et al., 2019; Lu et al., 2017; Lu et al., 2012; Niu et al., 2018; Shi et al., 2012; Tiejun et al., 2009; Yoon et al., 2001), transition metals (Fang et al., 2012; Kato et al., 2012; Nicholson et al., 2012; Ogo et al., 2012; Zheng et al., 2012), noble metals (Lu et al., 2017), rare earth ions (Huixian Shi et al., 2012), metal-organic frameworks (Buru et al., 2019; Ma et al., 2018; Stuckart and Monakhov, 2018), lanthanide series (Hu et al., 2012), cation exchange (Assran et al., 2012; Li et al., 2012; Qian et al., 2012; Tong et al., 2012), organometallic (Sokolov et al., 2012) and porous silica (Yahya et al., 2019).

Significantly, a critical and comprehensive review regarding practicality of Keggin-based POMs in environmental remediation, is still absent in the present context. Consequently, the current review can cast a light on structural tuning of the Keggin-based POM nanomaterials, conferring better charge separation, faster charge transfer, higher specific surface area, wider pH stability and higher recoverability in polar environment. To surmise, the significant previous research works on Keggin-based POMs photocatalysis have been critically reviewed herein. This encompasses strategized synthetic methods of Keggin-based POM nanocomposites, executable hierarchical enhancement and intensification process, and intelligible fundamental working principles. In addition to that, this review aims to shed a light on producing advanced Keggin-based POM nanocomposites with excellent photocatalytic properties in the near future.

2. Synthesis methods for Keggin-based polyoxometalate photocatalysts

The most commonly used methods to prepare Keggin-based POMs are chemical precipitation, sol-gel, wet impregnation, ultrasonication-assisted, sol-gel spin coating and hydrothermal. These synthetic techniques produce well-integrated Keggin-based POM nanocomposites with synergistic effects. A few other types of POMs, such as Preyssler and Wells-Dawson, are rarely reviewed. Despite that, an in-depth study of the design and synthesis of these

Table 1
The thermal stability of various commonly used POMs (Kozhevnikov, 1998).

POMs	Decomposition temperatures (°C)
$H_3PW_{12}O_{40}$ (PW)	465
$H_4SiW_{12}O_{40}$ (SiW)	445
$H_3PMo_{12}O_{40}$ (PMo)	375
$H_4SiMo_{12}O_{40}$ (SiMo)	350

POM nanocomposites are crucial in improving their structure-properties (Nur et al., 2014; Razali et al., 2014).

2.1. Chemical precipitation

One of the conventional and convenient approaches for producing Keggin-based POM photocatalysts is the chemical precipitation method. In this method, all the precursors are dissolve at room temperature or refluxing the mixture solution at the temperature around the boiling point of the solvent used (thermal treatment). This dissolution is followed by magnetic stirring for several hours to obtain the precipitate (product). Calcination is then performed in order to activate the photocatalysts by removing contaminants present on the surface of photocatalysts, eliminating organic directing templates, or enhancing the structural crystallinity. The calcination environments can be adjusted based on the characteristics of respective photocatalysts, some might be calcined under air flow, O_2/N_2 mixture flow or pure O_2 flow. Moreover, the calcination temperature could also become a consideration factor. This is because the decomposition of POM can cause a loss of activity; thus, their thermal stability needs to be studied. The thermal stability of commonly employed POMs is listed in Table 1.

Several researchers have adopted this method to synthesize the POM-based photocatalysts (Giannakoudakisa et al., 2019; Huang and Liu, 2020; Lan et al., 2016; Song et al., 2020). For examples, Lan and co-workers (Lan et al., 2016) had used this method to synthesize polyoxometalate (POM)@Co_3O_4 composites, accommodating a Keggin ion cluster into each confined space of a metal-organic-framework (MOF). They have developed a two-step, *in-situ* route in: (i) synthesis of POM@ZIF-67 and (ii) the subsequent calcination treatment (350 °C for 3 h) under air flow to produce (POM)@Co_3O_4. By adopting this chemical precipitation method, FESEM images showed that the POM@MOF retained similar pore size and smooth morphology of its surface. Furthermore, calcination at 350 °C was used to remove the organic compound. This can produce metal oxide framework to accommodate POM. The size of the framework can swing open and close to match with the size of the POM. This co-precipitation method is excellent in controlling the surface morphology and uniformity of the topology of the desired composites. The visible light driven photocatalytic activity was enhanced due to POM can accept electrons from porous Co_3O_4 and transfer the electrons to attack the substrate, in a confined, uniform cage of MOF. This electron transmission phenomenon can be further proven by using transient photocurrent response, as it exhibited an increase of photocurrent density when larger concentration of POM incorporated with Co_3O_4 in the MOF framework. This showed the electron storage ability of POM from the conduction band of Co_3O_4 could be enhanced with its concentration.

Huang and Liu Huang and Liu (2020) also utilized this chemical precipitation method to synthesize nanostructured carbon-doped ammonium phosphotungstate photocatalysts, using urea phosphotungstate (UPW) and thioureaphosphotungstate (TPW), whereby urea to HPW ratios were denoted as UPW, 3UPW, 5UPW; thiourea to HPW ratios were labelled as TPW, 3TPW and 5TPW. The phosphotungstate was mixed well with (i) urea and (ii) thiourea after chemical precipitation process. Nevertheless, low photocatalytic activities were observed for these series of composites. Subsequently, the calcination temperature at 390 °C for 4 h was implemented to polymerize carbon nitride onto phosphotungstate. It is found that all the listed ratios of urea/phosphotungstate hybrids and thiourea/phosphotungstate hybrids are different from their morphology appearance and chemical compositions. Urea carrying N-C═O and thiourea bearing N-C═S, both containing nitrogen atom, could form ammonium phosphotungstate. The visible light can be harvested by 5UPW and 5TPW, to photogenerate electrons (O^{2-}) at valence band to mid band gap of W5d conduction band, thus mixed valence POM may be formed. The photodegradation of imidacloprid was greatly enhanced (0.34 h^{-1} for 5UPW). Although chemical precipitation method is feasible under ambient condition, energy of bond breaking and bond forming at higher temperature is required to induce chemical interaction to improve the photocatalytic degradation efficiency. Besides this, considering the decomposition temperature of phosphotungstate, the calcination temperature should be kept below 465 °C (refer to Table 1); meanwhile, the polymerization of urea could be initiated.

2.2. Wet impregnation

Wet impregnation method is also extensively used in the preparation of POM-based photocatalysts (Jin et al., 2013; M and M, 2017; Tayebee et al., 2019; Wang et al., 2017; Zhang et al., 2020). This process involves mixing of two interactive phases: (i) homogeneous solution containing active metals, and (ii) solid phase containing solid support. The metals are dispersed onto the solid supports after stirring and followed by evaporation process. A past study showed that the phosphotungstic acid grafted SBA-15 was synthesized by blending phosphotungstic acid and SBA-15 at 40 °C for 30 min. After that, BiOBr solid was added into phosphotungstic acid/SBA-15 suspension. Then, the mixture solution containing BiOBr and phosphotungstic acid/SBA-15 was undergone 30 min mechanical stirring. Then, the mixture suspension was ultrasonicated for 30 min, and subsequently stirred for another 30 min. The stirring and ultrasonication processes were repeated thrice to ensure homogeneity. Finally, the suspension was evaporated at slightly high temperature, *i.e.* 60 °C for 4–5 h, and followed by vacuum drying for 10 h at 60 °C (Wang et al., 2017). This preparation method is time-consuming and tedious due to the repetitive steps of ultrasonification and mechanical stirring.

Due to some limitations of wet impregnation method, such as inhomogeneous distribution of active sites onto solid supports and weak physical interaction between two compounds, hence, an adhesive agent was commonly added (Zhang et al., 2020). Adhesive agent well functions as a bridge-mimicking intermediate to chemically crosslink two unmixable compounds into one composite associated with the changes in physio-chemical properties. Polyoxometalate ($(NH_4)_4[PMo_{11}VO_{40}]$)/graphitic nitride was successfully prepared by using sodium carboxymethyl cellulose (CMC) as an adhesive agent to link ($(NH_4)_4[PMo_{11}VO_{40}]$) and graphitic nitride together. Without CMC, POM and graphitic nitride might interact weakly as both compounds have high electron density; hence slight repulsion forces. CMC has negative ion, which can adhere to metal cations in the POM. Furthermore, hydroxyl group of CMC can also form hydrogen bonds with nitrogen tethered on the surface of graphitic nitride. The chemical interactions between ($(NH_4)_4[PMo_{11}VO_{40}]$) and graphitic nitride can be confirmed via FTIR absorption peaks, XRD diffraction peaks and DRS absorption bands. Based on infrared spectrum, Keggin POM displayed peaks at 782, 863, 960, 1109 and 1400 cm^{-1}. The functional groups of C-N and C═N of g-C_3N_4 stretched at 1100-1700 cm^{-1} while NH_2 or ═NH stretched at 3200 cm^{-1}. However, the bands were shifted after the integration of POM and graphitic nitride. Based on XRD diffratogram, the diffraction peak of g-C_3N_4 at 27.4° was weakened and POM at 26.4° was gradually decreased with increasing the amount of g-C_3N_4. The red-shifting of POM/g-C_3N_4 was also supported by DRS results, in which the absorption peak of g-C_3N_4 at 389 nm was slightly red-shifted to 391 nm after formation of POM/g-C_3N_4 (Please refer to Fig. 2). The performance of POM/g-C_3N_4 with 1:1 ratio showed degradation efficiency of 85.7%, 1:3 ratio yielded 94.7% and 1:5 ratio produced 91.5% degradation. The POM/g-C_3N_4 with 1:3 gave the best results among three of them.

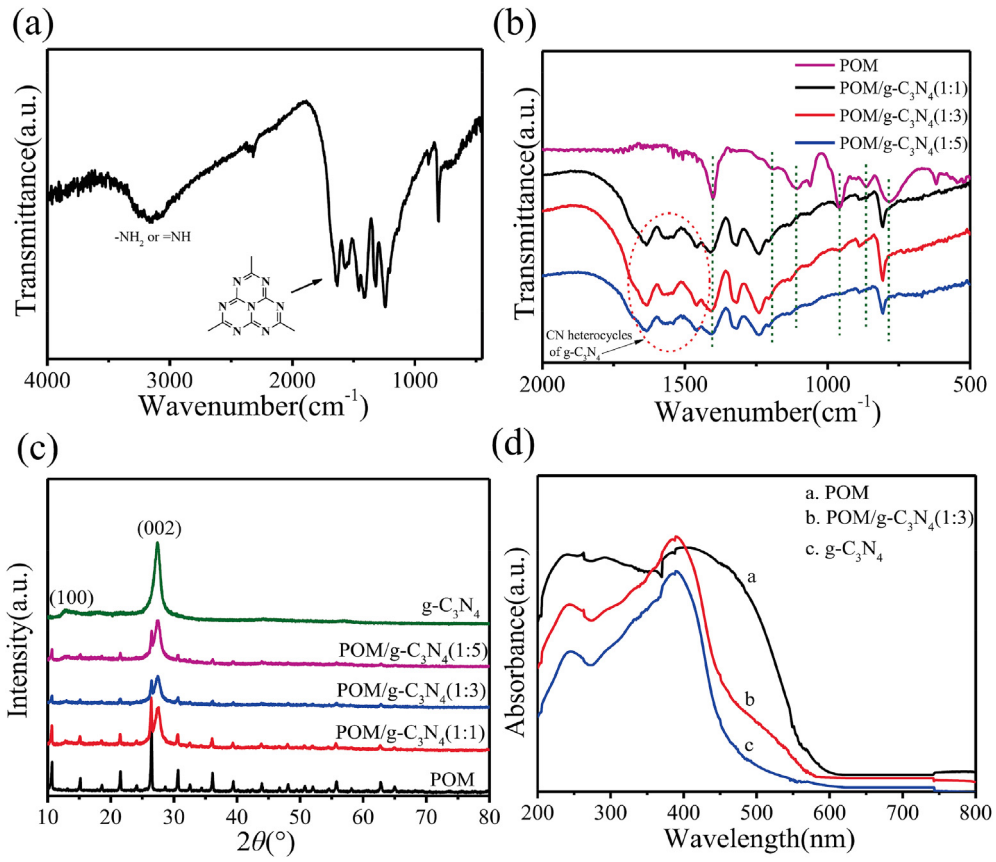

Fig. 2. (a) and (b) FTIR spectra; (c) XRD patterns and (d) DRS of different samples. Reprinted with permission from (Zhang et al., 2020). Copyright 2020 Elsevier.

However, POM/g-C_3N_4 with 1:5 unexpectedly showed poorer result which might due to the excessive presence of graphitic nitride that has blocked the POM's active sites (Zhang et al., 2020).

The same strategy was adopted by Kazemi et al. (Kazemi et al., 2018) whereby tetraorthosilicate (TEOS) firstly interacted with $NiFe_2O_4$ nanoparticles to form nanocomposites. Next, Keggin-based POM, $H_5PMoV_2O_{40}$, was functionalized onto tetraorthosilicate (TEOS)-$NiFe_2O_4$ nanoparticles to produce a magnetically-separable catalyst. TEOS acted as the adhesive agent to chemically link POM and $NiFe_2O_4$ by its hydroxyl groups. The Keggin-based POM was prepared by stirring and refluxing at 80 °C for 2 h. To ensure that TEOS has successfully form a bridge between Keggin-based POM and NiFe, FTIR is a tool to observe the bonding alteration. There is shifting of peak observed in the FTIR spectrum compared to the bare Keggin-based POM. Tayebee and co-workers (Tayebee et al., 2019) have also reported the same strategy as reported in (Kazemi et al., 2017) and (Zhang et al., 2020). They used 3-substituted indoles, *i.e.* 2-[(1H-indol-3-yl)(phenyl)methyl]malononitrile, as the linking intermediate between $H_3PW_{12}O_{40}$ and SBA-15. Due to the high dispersion of $H_3PW_{12}O_{40}$ over SBA-15, the result offered five-fold enhancement than that of the unsupported $H_3PW_{12}O_{40}$.

2.3. Sol-gel

Sol-gel method is known as a wet chemical method to fabricate, generally silica or titania, whereby the silica or titania sols (colloidal solution) gradually polymerize into gel-like network over a certain period of time. The hydrolysis of silica or titania source forms the sols, whereas polycondensation of silica or titania sols forms the gel. This method was also employed in the preparation of POM functionalized supports (Li et al., 2019; Sampurnam et al., 2018; Yahya et al., 2019). For instance, Yahya and co-researchers (Yahya et al., 2019) have successfully produced mesoporous aerogel silica/polyoxometalate hybrid employing sol-gel method under mild condition. The mesoporous aerogel silica was prepared by hydrolysis and condensation steps, subsequently, drying by CO_2 supercritical. POM was then functionalized onto mesoporous aerogel silica by methanol reflux for 3 h.

Another research group also reported a similar synthesis method to produce $H_3PW_{12}O_{40}/TiO_2$ composite film (Li et al., 2019). In order to ensure well dispersion of $H_3PW_{12}O_{40}$ in isopropanol, the solution was ultrasonicated for 10 min, then mixed thoroughly with titanium isopropoxide (TTIP). As we know, TTIP undergo fast hydrolysis and condensation in polar solvent, thus white suspension forms promptly, which indicating the large particles formed. With this reason, adding acetic acid is taken into account, to control the hydrolysis process of TTIP, in order to obtain small particle size of TiO_2. HCl was also added into the mixture solution so that $H_3PW_{12}O_{40}$ would not decompose easily under an acidic environment. The sol was subjected to hydrothermal at 200 °C in a Teflon-lined autoclave. This step produced hydrogel. Finally, the $H_3PW_{12}O_{40}/TiO_2$ composite film was obtained by spin-coating and aged for 7 days. A similar preparation method was also reported Lu et al. (2012). This work has applied programmed heating to obtain crystalline anatase TiO_2 at temperature, *i.e.* 200 °C. Sols was transferred into a Teflon-lined autoclave (473 K, 2 K min^{-1} heating rate) for 2 h heating. After that, the hydrogel was stirred for spin-coating to form composite film. Conventionally, temperatures from 400 to 500 °C, are essential to initiate the crystallization of

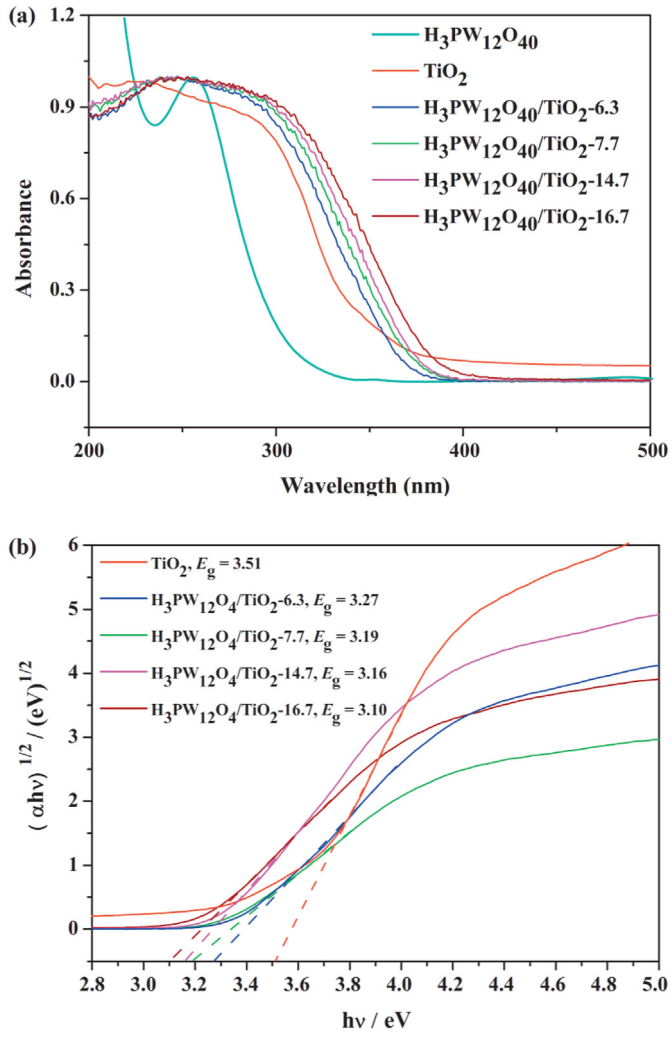

Fig. 3. UV–vis/DRS of (a) absorption bands and (b) band gaps of the starting $H_3PW_{12}O_{40}$, as-prepared pure TiO_2 film, and $H_3PW_{12}O_{40}/TiO_2$ composite films with different $H_3PW_{12}O_{40}$ loadings. Reprinted with permission from (Lu et al., 2012). Copyright 2012 Elsevier.

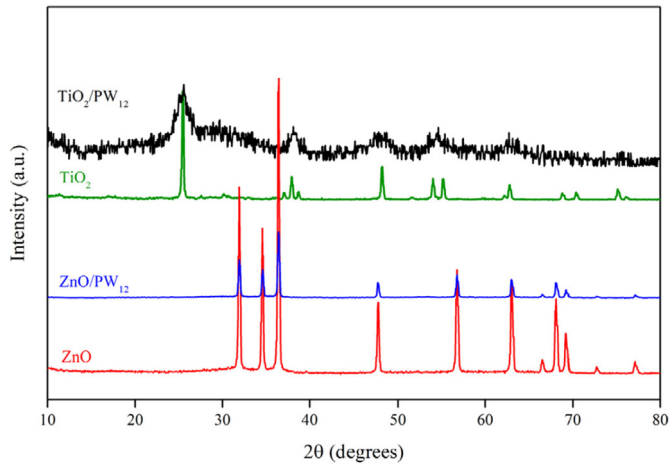

Fig. 4. XRD patterns of bare TiO_2 and ZnO, TiO_2/PW_{12} and ZnO/PW_{12} nanocomposite. Reprinted with permission from (Taghavi et al., 2018). Copyright 2018 Elsevier.

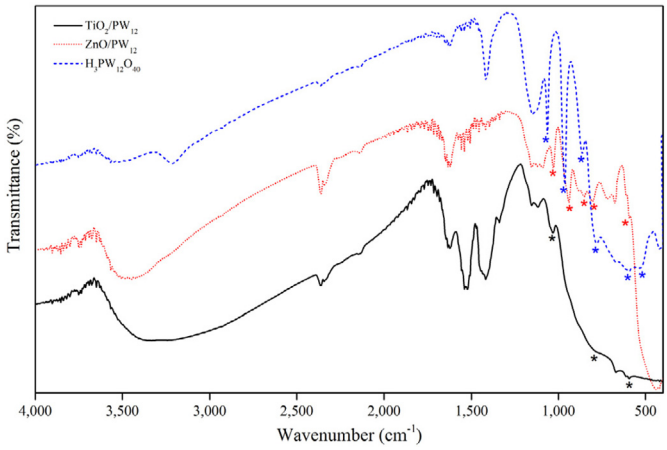

Fig. 5. The FT-IR absorption spectrum of TiO_2/PW_{12} and ZnO/PW_{12} nanocomposite. Reprinted with permission from (Taghavi et al., 2018). Copyright 2018 Elsevier.

TiO_2 at anatase phase; however, it was found that the programmed heating rate could be manipulated to obtain crystalline, anatase TiO_2 at lower heating temperature, *i.e.* 200 °C. In contrast, amorphous TiO_2 was obtained at 200 °C when there was no gradual increment of transient heating temperature Guo & Hu, 2007.

$H_3PW_{12}O_{40}/TiO_2$ composite films with their characteristics, such as crystallinity, chemical interaction, surface area, textural morphology, were studied and discussed as follows (Lu et al., 2012). The crystallinity of $H_3PW_{12}O_{40}/TiO_2$ composite films was remained intact as pure TiO_2 film, it might owing to $H_3PW_{12}O_{40}$ incorporation into TiO_2 polymeric framework, thus forming one homogeneous anatase composite. On the other hand, Taghavi and co-workers (Taghavi et al., 2018) have done the similar work. The diffraction peaks of base TiO_2 display tetragonal anatase with high crystallinity after the hydrothermal treatment. However, the crystallinity of the $TiO_2/H_3PW_{12}O_{40}$ decreases compared to pure TiO_2. This can be attributed to the $H_3PW_{12}O_{40}$ distribution over TiO_2 anatase framework, thus retarding its anatase crystallinity development.

Fig. 3(a) and (b) illustrates the absorption peaks and band gaps of TiO_2 and of $H_3PW_{12}O_{40}/TiO_2$ films with a series different amount of $H_3PW_{12}O_{40}$. Apparently, increasing amount of $H_3PW_{12}O_{40}$ could shift the absorption peak of TiO_2 to a longer wavelength. It is proven that the bandgap of TiO_2 and $H_3PW_{12}O_{40}/TiO_2$ have been narrowed and thus, more photogenerated electrons could reach the conduction band easily and then adsorbed by O_2 from the surrounding (Lu et al., 2012).

Based on literature (Taghavi et al., 2018), there is no peaks of $H_3PW_{12}O_{40}$ noticed in XRD diffractograms of $TiO_2/H_3PW_{12}O_{40}$ and $ZnO/H_3PW_{12}O_{40}$, but there is a decrease in crystallinity (Please refer to Fig. 4), this is due to the reason mentioned beforehand. FTIR was employed to distinguish the presence of $H_3PW_{12}O_{40}$. Evidently, IR spectrum of $ZnO/H_3PW_{12}O_{40}$ nanophotocatalyst in Fig. 5 shows the absorption band of δ(O-P-O) at 592 cm^{-1}. Moreover, shifting and broadening the band shapes of $TiO_2/H_3PW_{12}O_{40}$ and $ZnO/H_3PW_{12}O_{40}$ are definitely confirmed Keggin-based POMs are chemically functionalized onto ZnO/TiO_2 support. The aniline photodegradation efficiency in the presence hydrogen peroxide, $TiO_2/H_3PW_{12}O_{40}$ or $ZnO/H_3PW_{12}O_{40}$ improved when it was compared to bare TiO_2 and ZnO under UV irradiation.

Significantly, Huixian Shi and co-researchers (Shi et al., 2012) have enhanced the photocatalytic activity of TiO_2 loaded rare ions (La^{3+} and Ce^{3+}) and POM under UV light irradiation, with the denotations as Ce-$H_3PMo_{12}O_{40}/TiO_2$ and La-$H_3PMo_{12}O_{40}/TiO_2$ composites. Sol-gel synthesis was employed and the nanocomposites

were calcined at different temperatures (400, 500, 600, 700, 900 °C) to enhance the anatase phase of TiO_2, proven by XRD diffraction peaks. It is discovered rare earth ions could act as a Lewis acid to accept electron pairs from Lewis base, *i.e.* adsorbed O_2, to form complexes. Thereto, embedding rare earth ions into semiconductors could enhance the charge separation and hence, reducing the charge recombination possibility of the photocatalyst. Furthermore, the light absorption of the semiconductor can be extended, shown by UV−vis DRS spectra. These effects can promote the photodegradation rates as reported in previous literature, *i.e.* La-TiO_2 (Huang et al., 2017), Nd-TiO_2 (Rengaraj et al., 2007), Pr-TiO_2 (Chiou and Juang, 2007). The same effect of light extension also conferred towards POMs. It is suggested that researchers may explore the rare earth ions doped with $TiO_2/H_3PW_{12}O_{40}$ under visible light illumination since several characteristics presented by this combination is very convincing in this direction.

The last synthesis method that is introduced here is reported by Nan Lu and co-researchers (Lu et al., 2017). The employed approach is the coupling of sol-gel and hydrothermal syntheses. It is the similar procedures mentioned beforehand (Li et al., 2019). The purpose of coupling these two approaches is to enhance the crystallinity of TiO_2 in the programmed heating process (2K min^{-1}, heated up to 200 °C for 2 h) of hydrothermal method, whereas as sol-gel's role is to ensure titanium tetraisopropoxide (TTIP) was well mixed with $H_3PW_{12}O_{40}$ and silver nitrate ($AgNO_3$) in the solution. Besides this, slowing down the hydrolysis and polymerization process of TiO_2 has been taken into account; thereby, acetic acid was added in TTIP solution. In addition, HCl (2 Molarity) was also added in the TTIP solution to control the pH lowering down to 2 to 3. It is owing to $H_3PW_{12}O_{40}$ can remain its structural stability, without decomposition, at the acidic condition. Sol was formed after stirring TTIP, $H_3PW_{12}O_{40}$ and $AgNO_3$ for an hour; subsequently, hydrogel was formed after the mixture solution was programmed heated for 2 h in Teflon-lined autoclave. Despite this, composite film is recently considered as a better choice compared to powder form, due to the film is ease in separation of photocatalyst from the pollutants. Hence, spin-coating was adopted to transform the hydrogel into composite film, which was undergone 7 aging days prior to get a dried composite film for photocatalytic testing. The photocatalyst formed was Ag-$TiO_2/H_3PW_{12}O_{40}$.

Based on literature (Lu et al., 2017), the characterization data are discussed here. There are several proofs of Ag, TiO_2 and $H_3PW_{12}O_{40}$ were homogeneously dispersed. This Ag-$TiO_2/H_3PW_{12}O_{40}$ composite film showed a very smooth surface morphology compared to $TiO_2/H_3PW_{12}O_{40}$ based on FESEM images. The lattice fringes of TiO_2, 0.35 nm (101) and Ag, 0.236 nm (111) were clearly depicted side-by-side in TEM image. In XPS spectra, the shifting of $TiO_2/H_3PW_{12}O_{40}$ compared to bare TiO_2 spectra showed that TiO_2 and $H_3PW_{12}O_{40}$ were chemically interacted (Ti-O-W) to form $TiO_2/H_3PW_{12}O_{40}$. The crystallinity of bare TiO_2 was considerably high but it was decreased after bonded to Ag. It is worth noting that cubic Ag has the ability to retard the crystallinity growth of anatase TiO_2. The narrow band gap was proven by the combination of TiO_2 and $H_3PW_{12}O_{40}$ with a slight red-shift of DRS absorption peak. Nonetheless, the electron-hole recombination rate can be further improved by adding Ag. It is note-worthy that Ag is responsive to photons and causes surface plasmon resonance (SPR). The oscillating of electrons can enhance the electromagnetic field of Ag and create potential energy difference between Ag and TiO_2. This could result in the oscillating electrons of Ag flow to conduction band of TiO_2 and hence, remaining the charge separation effect. This effect were proven by Surface-Enhanced Raman Scattering (SERS), TEM and UV−Vis DRS.

To conclude literature studies on sol-gel synthesis, it is extensively used to prepare POM-based nanocomposites, meanwhile coupling with another assisted methods, including hydrothermal reaction in an Teflon-lined autoclave, ultrasonication, calcination, spin-coating and so forth, to ensure the design and structure of the resulting product are strictly achieved. Undeniably, sol-gel is an excellent method in tuning the morphology and topology of composites, yet it presents some limitations too. For an example, it takes several days or weeks for hydrogels to under aging process. Then, the aged gel will be calcined at high temperature or evaporated at 60 °C under vacuum condition, to yield solid powder. To overcome this shortcoming, there are also other methods have been evaluated in recent years, such as photopolymerisation (Ghali et al., 2019), *in situ* hot-pressing synthesis method (Li et al., 2019), carbonization method (Ramalingam et al., 2019) and photodegradation of surfactant template (Zi et al., 2016). Moreover, it is obvious that sol-gel and hydrothermal are inseparable approaches to prepare composites. It is owing to the Teflon-lined autoclave with hydrothermal temperature ranging from 150 to 200 °C, could produce well dispersed mixture solution and chemically interacted, even to induce crystallinity of TiO_2/POM when heating rate is applied. Nonetheless, the Teflon-lined autoclave has its reaction temperature limitation, with not exceeding *ca.* 200 °C. Considering this deficiency in the hydrothermal treatment, polypropylene (PPL)-lined autoclave could be used to replace Teflon-line autoclave if the desired hydrothermal temperature is more than 200 °C, but less than or equal to 300 °C.

Here, we summarized key findings from the various synthesis techniques employed for the preparation of Keggin-based POM nanocomposites:

1. Chemical precipitation is a feasible and convenient method as all the precursors are prepared in *one-pot* to obtain the solid precipitates. The obtained solids are generally good in surface morphology and topology. Nonetheless, some precaution steps, such as mixed ratios of precursors, heating temperature, preparation duration, *etc.*, have to be taken into account, as these are crucial to achieve the desired morphology and topology.
2. Impregnation is a simple method. It involves mixing of solid supports and solution containing active metals to form a solid product; nonetheless, it does not yield homogeneous dispersed metals on the solid supports. To overcome this shortcoming, the solid support and the solution may be linked by an adhesive, which can chemically bond to both of them.
3. Sol-gel-hydrothermal is generally favored by researchers in the synthesis of POM photocatalysts. In spite of this, it is quite time consuming and uneventful. Thus, other approaches such as polymerization, carbonization, *in-situ* hot pressing methods could be adopted too. Other than this, to increase the hydrothermal temperature, the Teflon-lined autoclave can be replaced by Polypropylene-line autoclave.

Other assisted methods, such as ultrasonication, spin-coating, calcination, evaporation, and vacuum drying also act as the complementary tools for the abovementioned approaches.

The data and descriptions by different research groups are actually in agreement with each other. Detailed discussion of optical properties is presented as below because it is the vital factor to relate to photochemical behaviour (photoinduced charge separation and charge transfer), which can enhance the practicality and photodegradation efficiency. Other physicochemical properties are also exhibited and summarized in brief to show the homogeneous integrity of the POM binary and ternary structures. Below are the recapitulations of the main characterizations of Keggin-based POM photocatalysts:

1. Optical properties (DR UV–vis, Photoluminescence and Electrochemical Impedance analyses): The characteristic charge transfer absorption band ($O^{2-} \rightarrow W_{5d}$) of Keggin-based POM is around 260–270 nm and edge absorption at *ca.* 380 nm (Huang et al., 2017; Yang et al., 2012) but it could be red-shifted to region 600 nm after immobilization of PW_{12} onto SiO_2 support, with a hump appeared at 440–450 nm due to charge transfer of O^{2-} to SiO_2. The extended absorption is varied depending on the types of support. For instances, the edge of g-C_3N_4 was extended from 500 to 580 nm (Zhang et al., 2020) whereas graphene oxide absorption edge was redshifted from 500 to 520 nm (Liu et al., 2018). Additionally, PMo_{12}/TiO_2 absorption band displayed at 400 nm, but it redshifted to 900 nm after Pt photodeposited onto PMo_{12}/TiO_2 composite. This effect was attributed to the surface plasmon resonance of Pt nanoparticles, causing narrower bandgap with 3.177 eV, compared to PMo_{12}/TiO_2 composite, 3.242 eV. Photoinduced charge separation and charge transfer of $Pt/PMo_{12}/TiO_2$ were enhanced compared to PMo_{12}/TiO_2 and TiO_2, shown by photoluminescence and electrochemical impedance spectra (Shi et al., 2019). Ag_3PO_4/PW_{12}/Graphene Oxide (Liu et al., 2018) reported by Guodong Liu and his co-researchers also showed the similar discovery as previous (Shi et al., 2019). It could be observed that $Pt/PMo_{12}/TiO_2$ and Ag_3PO_4/PW_{12}/Graphene Oxide triads have lower intensity in the spectra compared to PMo_{12}/TiO_2 and Ag_3PO_4/PW_{12} dyads, implying the photogenerated electrons are transmitted from binary composites to Pt or Ag, respectively. This can enhance charge separation and charge transfer, hence photoinduced charge recombination could be retarded.
2. Chemical interaction (FTIR analysis): Keggin-based POMs generally presented four to five characteristic bands at region from 800 to 1200 cm^{-1}, including (Taghavi et al., 2018; Zhang et al., 2020):
   (i) $H_3PW_{12}O_{40}$: P-O 1080 cm^{-1}, O-P-O 596 cm^{-1}, $W{=}O_{terminal}$ 981 or 985 cm^{-1}, $W\text{-}O_{corner}\text{-}W$ 890 cm^{-1}, $W\text{-}O_{edge}\text{-}W$ 805 cm^{-1}; and
   (ii) $H_3PMo_{12}O_{40}$: P-O 1080 cm^{-1}, O-P-O 596 cm^{-1}, $Mo\text{-}O_{edge}\text{-}Mo$ 782 cm^{-1}, $Mo\text{-}O_{corner}\text{-}Mo$ 863 cm^{-1}, $Mo{=}O_t$ 960, 1109 and 1400 cm^{-1}.

However, the chemical compounds, such as SiO_2 (IR absorption band *ca.* 960 to 1100 cm^{-1}), with their bands at around that region might mask these POM characteristic bands. Besides, we can notice that the band shifting might occur if there is chemical interaction between POM and supported materials.

3. Crystallinity (XRD analysis): The crystallinity of Keggin-based POM could be weaken but without fully disappearing. This proves that the chemical interaction happens once it has successfully functionalized with other chemical compounds. In other case, the peaks of POM might be totally disappeared, owing to the well dispersion of POM into the supports.
4. Surface area (BET analysis): Keggin-based POM surface is generally reported less than 10 $m^2\ g^{-1}$, however, it could be increased up to 200 $m^2\ g^{-1}$ after immobilized with supports. The surface areas are varied according to the types of the supports.

Table 2 summarizes preparation methods, physicochemical properties and photocatalytic efficiencies of Keggin-based POMs.

3. Hierarchical enhancement of Keggin-based polyoxometalate photocatalysis

POM-based materials have been widely lauded for excellent photocatalytic effects attributed to their preeminent photoelectrochemical properties, tailorable physicochemical properties, condensed redox density and strong acidity persistency. With proper settings, complete mineralization can even be achieved with zero-waste establishment. Despite, their practicalities are highly hampered by the high tendency of bare POM in structural dissociation in water and narrow light absorption range. In order to tackle the drawbacks of POM materials, various techniques were applied to maximize the degradation efficiency for practicality prospect. Current section focuses on the techniques endeavored recently, ranging from modification of POM-based photocatalyst to process intensification, subsequently achieving the enhanced photocatalytic efficiency and structural stability; hence the practicality of POM photocatalysis.

3.1. Modification of Keggin-based polyoxometalate photocatalysts

As aforementioned, one of the major restrictions faced by POM materials in heterogeneous photocatalysis is the tendency of structural dissociation in substrate solution, causing secondary pollution in addition to losses in photocatalytic activity. Considering the recyclability and practicality prospects, a lot of efforts were attempted, including *in-situ* solid phase thermal transformation (Huang and Liu, 2020; Meng et al., 2019), coupling with semiconductors (Tang et al., 2020; Wu et al., 2020; Zhou et al., 2019), immobilization onto selected supports (Farhadi and Zaidi, 2009; Guo et al., 2000; Kumar & Landry, 2007; Yue et al., 2002), magnetization via Fe-based material for facile separation (Qiu et al., 2007; Shi et al., 2006; Yu et al., 2019; Zhang et al., 2017). All these modifications attempt to improve POM-photocatalysis from following aspects: enhancements of performance and structural stability, as well as facile post-reaction separation, for the sake of practicality of POM-photocatalysis.

It is known that photocatalytic performance of POM is closely associated to its optical properties. To enhance the light-harvesting ability, Meng and co-workers (Meng et al., 2019) engineered the stacked-layer carbonitride/tungstophosphate (TCN) via solid-state conversion of melamine phosphotungstate (MPW). Typically, dissolved phosphotungstic acid hydrate (HPW) was mixed with melamine solution, then subjected to heating, washing, and drying to obtained white solid powder prior to calcination process. The obtained photocatalysts exhibited better light absorbability as opposed to bare constituent (carbonitride (CN)) prepared under similar outline, attaining 13.5 times of photoactivity enhancement the coupling of POM-material (tungstophosphate). Specifically, around 80% of imidacloprid removal was achieved after 6 h of visible light irradiation (225 W) in the presence of 2 g/L of optimized photocatalyst (13TCN, whereby 13 is denoted for mol ratio of melamine to HPW). However, a gradual loss of photocatalytic activity was observed after 3 recycle of photoreaction, mainly attributed to the blockage of active sites by the substrates and intermediate.

The instability of the above POM-based photocatalyst can be improved by switching the carbon-based precursor to urea. Huang and Liu Huang and Liu (2020) synthesized a series of urea phosphotungstate (UPW) photocatalysts with the similar outline, except changing the carbon-based precursor from melamine to urea. Similarly, all the POM photocatalysts exhibited enhanced photocatalytic effects in degrading imidacloprid. Compared to melamine-synthesized photocatalyst, current urea-synthesized UPW recorded similar imidacloprid removal of 76.30% with only 3 h of visible light irradiation, even with lesser chemical needed during photocatalyst synthesis (urea to HPW ratio of 5). Authors claim that the carbon content incorporated in the 5UPW (5 denotes for ratio of precursors) optimally extended the absorption range towards the

Table 2
Preparation methods, physicochemical properties and photocatalytic efficiencies of Keggin-based POMs were summarized.

Composites	Synthesis methods	Physicochemical properties	Photocatalytic reactions	Substrates or pollutants	Photocatalytic efficiencies	References
$((NH_4)_4[PMo_{11}VO_{40}])/g\text{-}C_3N_4$	Dipping method with wet impregnation (no thermal treatment); sodium carboxymethyl cellulose (CMC) as adhesive	• Absorption bands of POM were at 240 and 404 nm; while $g\text{-}C_3N_4$ was in the range of 200 −500 nm. After POM templated with $g\text{-}C_3N_4$, new hump appeared at 389−391 nm and the absorption edge at 500 nm was extended to 580 nm	•300 W Xenon lamp •Visible light irradiation	• Methylene Blue (MB) • X−3B	• 94.7% in 120 min ($0.79\ min^{-1}$)	(Zhang et al., 2020)
Carbon-doped $H_3PW_{12}O_{40}$ UPW = urea phosphotungstate; TPW = thiourea phosphotungstate	Co-precipitation and thermal treatment (inert calcination at 390 °C); Carbon sources consisted of urea and thiourea	• Bare HPW band gap was recorded at 3.4−3.6 eV; 5UPW-390 band gap at 3.16 eV; 5TPW-390 band gap: 3.14 eV, inferring the bandgap was narrowed with urea and thiourea interrupted the bandgap of bare HPW. • Mid gap states exhibited upon carbon doping, shown by photoluminescence spectrum.	•225 W Xenon lamp •Visible light irradiation	• Imidacloprid	• 76.29% ($0.34\ h^{-1}$) • Photocatalytic reaction was recycled for three times consecutively with similar photodegradation efficiency	Huang & Liu, (2020)
$[H_5O_2]_2[Hpip]_{2.5}[BW_{12}O_{40}].4H_2O$ or protonated piperazine POM Pip = piperazine, $C_4H_{10}N_2$	Co-precipitation with refluxing	• N-H group of Pip and O atoms in POM can be linked together via hydrogen bonding, proven by FTIR vibration shifting of N-H and C-H in the organic-inorganic POM.	•200 W LED lamp; •Visible light irradiation	• Methylene Blue (MB)	• 97.08% after 24 min ($4.05\ min^{-1}$) • Photocatalytic reaction was recycled for five times consecutively with similar photodegradation efficiency	Jamshidi et al. (2020)
$Pt/H_3PMo_{12}O_{40}/TiO_2$ nanofibers $PMo_{12} = H_3PMo_{12}O_{40}$	$H_3PMo_{12}O_{40}/TiO_2$ by electrospinning, calcination at 450 °C and followed by Pt photoreduction or photodeposition.	• PMo_{12}/TiO_2 absorption band displayed at 400 nm, but it redshifted to 900 nm after Pt photodeposited onto PMo_{12}/TiO_2 composite. This effect was attributed to the surface plasmon resonance of Pt nanoparticles. • Pt nanoparticles presented localized surface plasmon resonance to PMo_{12}/TiO_2 causing narrower bandgap with 3.177 eV, compared to PMo_{12}/TiO_2 composite, 3.242 eV. • Photoinduced charge separation and charge transfer of $Pt/PMo_{12}/TiO_2$ were enhanced compared to PMo_{12}/TiO_2 and TiO_2, shown by photoluminescence, transient photocurrent responses and electrochemical impedance spectra.	•300 W Xenon lamp •Visible light irradiation	• Methyl Orange (MO) • Tetracycline • Bisphenol A	• Photodegradation efficiencies of Methyl Orange, $0.011\ min^{-1}$; Tetracycline, $0.043\ min^{-1}$; Bisphenol A: $0.00615\ min^{-1}$ • The similar photodegradation efficiencies shown after recycling five times consecutively	(Shi et al., 2019)
$H_3PMo_{12}O_{40}$/polymer $SiMo_{12}O_{40}(IPh_2)_4$/polymer	Photopolymerisation of TMTPA monomer under visible light	• TMPTA with the aid of photoinitiator and iodonium salt to form polymer. The	• LED@375 nm • UV irradiation	• Eosin-Y	• 93% of Eosin-Y was degraded by $H_3PMo_{12}O_{40}$/polymer	Ghali et al. (2019)

(*continued on next page*)

Table 2 (*continued*)

Composites	Synthesis methods	Physicochemical properties	Photocatalytic reactions	Substrates or pollutants	Photocatalytic efficiencies	References
Polymer: poly(TMTPA) = poly(trimethylolpropane triacrylate)		intensity of TMPTA in infrared spectra was reduced after undergone polymerization process.			in 87 min (1.069 min^{-1}); meanwhile, degraded by $SiMo_{12}O_{40}(IPh_2)_4$/in 200 min (0.465 min^{-1})	
$H_3PW_{12}O_{40}$@MFM-300(In) composites MFM-300(In) is a type of MOF synthesized by $In(NO_3)_3.5H_2O$ and biphenyl-3,3′,5,5′-tetracarboxylic acid	*In-situ* hot-pressing, solvent free synthesis	• $H_3PW_{12}O_{40}$@MFM-300(In) absorption edge was stretched out to 450 nm compared to MFM-300(In) and new band appeared at 550–600 nm due to oxygen in POM exhibited charge transfer to In(III) in MOF. • Photoluminescence spectra showed the intensity of MFM-300(In) decreased after interaction with PW_{12}, implying efficient electron transfer from MFM-300(In) to PW_{12}. • UV–vis spectra proved there is no POM leaching after the composite recycled several times. • PXRD pattern proved the structure of the composite remain intact after eight consecutive cycles	• Visible light irradiation • H_2O_2 was added as an initiator	• Sulfamethazine	• 98% degradation activity in 120 min (0.82 min^{-1}) • 85% of photodegradation efficiencies shown after recycling eight times.	(Li et al., 2019)
$[Cd(TTPB\text{-}4)(DMF)_3]_4[PMo_{12}O_{40}]_2[HPMo_{12}O_{40}].6DMF.4H_2O$ TTPB-4 = 1,3,5-tris(4-(4H-1,2,4-triazol-4-yl) phenyl)benzene]	Hydrothermal synthesis	• TTPB is a ligand, acting as an electron shuttler, to transfer electrons to POM, as proven by the photoluminescence result showing a reduced intensity of TTPB after coupling with POM. • POM guest interconnected with MOF via TTPB-4 can give a very stable and confined framework.	• 500 W Xenon lamp; • H_2O_2 as the oxidant; • UV irradiation	• Crystal Violet (CV) • Basic Red 2	• Crystal Violet: 94.3% in 36 min (2.62 min^{-1}); • Basic Red 2: 95.0% in 18 min (5.27 min^{-1}) • Photocatalytic reaction was recycled for three times consecutively with similar photodegradation efficiency.	(Liu et al., 2018)
TiO_2/POM/Fe_3O_4@SiO_2 microspheres $PW_{12} = H_3PW_{12}O_{40}$ $SiW_{12} = H_4PSi_{12}O_{40}$ $PMo_{12} = H_3PMo_{12}O_{40}$	$TiO_2/H_3PW_{12}O_{40}$ thin film was constructed by electrostatic layer-by-layer method onto Fe_3O_4@SiO_2 microspheres	• Low degradation efficiency of Fe_3O_4@SiO_2@$(TiO_2/SiMo_{12})_{10}$ is due to the reduction potential of its reduced form is more positive than O_2/O_2^-, so itself is hard to re-oxidized and reused. • Synergistic effect of POM/TiO_2 could be proven by improvement of quantum efficiency, in which photoinduced electrons transferred from conduction band of TiO_2 to POM and thus, retarding the recombination process.	• 300 W medium-pressure Mercury lamp • Inorganic oxidants were used, including $KClO_3$, $KBrO_3$ and KIO_3. • UV irradiation	• Methylene Orange (MO)	• Fe_3O_4@SiO_2@$(TiO_2/PW_{12})_{10}$ degraded 83.91% of MO in 100 min (0.84 min^{-1}). • Fe_3O_4@SiO_2@$(TiO_2/SiW_{12})_{10}$ degraded 62.07% of MO in 100 min 0.62 min^{-1}). • Fe_3O_4@SiO_2@$(TiO_2/SiMo_{12})_{10}$ degraded 13.55% of MO in 100 min (0.14 min^{-1}).	Niu et al. (2018)

$Ag_3PO_4/PMo_{12}/GO$ GO = Graphene Oxide; $PMo_{12} = H_3PMo_{12}O_{40}$	One-pot approach with chemical precipitation	• Due to the reduction potential of Ag_3PO_4 is more negative than PMo_{12}, thus PMo_{12} can fast capture electrons from Ag_3PO_4. • PMo_{12} and GO were introduced into Ag_3PO_4 to enhance the charge transfer and separation of Ag_3PO_4, proven by low intensity of photoluminescence and electrochemical impedance spectra. • Bandgap of Ag_3PO_4 was 2.40 eV, however it was narrowed to 2.10 eV after combined with PMo_{12} and GO.	• 500 W Xenon arc lamp • Solar light irradiation	• Rhodamine-B (RhB)	• RhB was degraded by Ag_3PO_4 at 0.1 min^{-1}, Ag_3PO_4/POM at rate of 0.15 min^{-1} and Ag_3PO_4/POM/GO at rate of 0.18 min^{-1}.	(Liu et al., 2018)
$TiO_2/H_3PW_{12}O_{40}$ ZnO/$H_3PW_{12}O_{40}$	Sol-gel and Teflon-lined hydrothermal treatment	• Integrity of the binary composites were studied using XRD and FTIR.	• 11 W low-pressure Mercury lamp • UV irradiation	• Aniline	• Aniline degraded by TiO_2/PW_{12} at rate $0.28X10^{-2}$ min^{-1}; by ZnO/PW_{12} at rate $0.26X10^{-2}$ min^{-1}	Taghavi et al. (2018)
$H_3PW_{12}O_{40}/SiO_2$ sensitized by H_2O_2	Sol-gel and thermal heating (calcination) at 200 °C for 4 h	• Absorption band of bare $H_3PW_{12}O_{40}$ depicted at 260 nm and its edge at 380 nm, but it was extended to around 600 nm after $H_3PW_{12}O_{40}$ functionalized with SiO_2.	• 500 W Xenon lamp • Solar light irradiation	• Methyl orange • Methyl red • Methyl violet • Rhodamine-B • Malachite green • Methylene blue	• Degradation efficiencies were ranging from 84.6% to 98.3% in 120 min (0.705—0.819 min^{-1}).	(Huang et al., 2017)
Ag-$TiO_2/H_3PW_{12}O_{40}$ composite film	Sol-gel and spin coating	• Compared to TiO_2, Ag-TiO_2, $TiO_2/H_3PW_{12}O_{40}$, electrochemical impedance spectra showed that Ag-$TiO_2/H_3PW_{12}O_{40}$ composite film displayed the smallest arc radius, indicating it has the least charge transport resistance. • Ag-$TiO_2/H_3PW_{12}O_{40}$ composite film displayed a weak and broad band from 400 to 500 nm, which is due to surface plasmon effect of Ag to accept transported electrons from hybrid $H_3PW_{12}O_{40}$ and TiO_2.	• 300 W Xenon lamp • Solar light irradiation	• *O*-chlorophenol (*O*-CP)	• 82.40% *O*-CP was degraded by Ag-$TiO_2/H_3PW_{12}O_{40}$ composite film in 240 min-1 (0.34 min^{-1}) • The composite film remained structural stable with 80% above degradation efficiency after three consecutive recycling used.	Lu et al. (2017)
La-$H_3PW_{12}O_{40}/TiO_2$ Ce-$H_3PMo_{12}O_{40}/TiO_2$	Sol-gel and thermal heating (calcination) at 400, 500, 600, 700 and 900 °C for 3 h respectively	• Specific surface area of TiO_2 was increased from 30 to 72 −74 m^2 g^{-1} after it was incorporated to form La-$H_3PW_{12}O_{40}/TiO_2$ Ce-$H_3PMo_{12}O_{40}/TiO_2$. • Anatase TiO_2 can be obtained by calcination up to 600 °C, however, further higher calcinated temperature can form rutile TiO_2 caused a	• 125 W high pressure Mercury lamp • UV light irradiation	• Methylene blue	• 96% MB was degraded by Ce-$H_3PMo_{12}O_{40}/TiO_2$ (0.96 min^{-1}) and 98% was degraded by La-$H_3PW_{12}O_{40}/TiO_2$ (0.98 min^{-1}) in 100 min respectively.	(Shi et al., 2012)

(*continued on next page*)

Table 2 (*continued*)

Composites	Synthesis methods	Physicochemical properties	Photocatalytic reactions	Substrates or pollutants	Photocatalytic efficiencies	References
		decreased in degradation efficiency. •Bandgaps of La-$H_3PW_{12}O_{40}$/TiO_2 and Ce-$H_3PMo_{12}O_{40}$/TiO_2 were reduced compared to TiO_2, due to *f* electrons of rare earth ions and TiO_2 having charge transfer to-and-fro at visible region.				
$H_3PW_{12}O_{40}$/TiO_2	Sol-gel and programmed temperature (200 °C) hydrothermal synthesis	• Local environment of $H_3PW_{12}O_{40}$/TiO_2 was broad at the region 200–450 nm, compared to sharp peak of $H_3PW_{12}O_{40}$ at 280 nm and 200–300 nm of TiO_2 band. • Programmed temperature at 200 °C successfully induced anatase TiO_2 incorporated with $H_3PW_{12}O_{40}$, which the crystallinity of TiO_2 and electron storage ability of PW_{12} could enhance the waste degradation efficiencies.	• 400 W Xenon lamp • Visible light irradiation	• Congo Red (CR) • Methyl Orange (MO) • Ponceau G (PG) • Orange II (OII) • Eriochrome Blue Black B (EB) • Alizarin S (AS) • Methylene Bule (MB) • Neutral Red (NR) • Rhodamine B (RB) • Fusin Acid (FA)	Degradation efficiencies of the substrates are shown below: • CR: 92% in 2 h • MO: 72.4% in 4 h • PG: 94.8% in 3 h • OII: 67.2% in 4 h • EB: 75.8% in 3 h • AS: 72.8% in 4 h • MB: 96% in 1 h • RB: 98% in 1 h • FA: 75% in 4 h	(Yang et al., 2005)

visible light region, hence effectively enhanced the photodegradation efficiency. Despite having more carbon content, 8UPW does not display a better photocatalytic activity, owing to the blockage of photo-active sites induced from excess carbon species doped on the surface of photocatalyst. Compared to the above study (Meng et al., 2019), the performance stability of urea-doped POM photocatalyst in present study is greatly enhanced, whereby the degradation efficiencies maintained at ~70% even after three consecutive of photoreaction. However, the reason of improvement in term of performance stability is not mentioned in the report.

In addition, the structural and performance stabilities can also be enhanced via coupling with other semiconductors. Similar with POM material, implementation of CdS photocatalyst in visible light region is highly suppressed by the structural instability upon photon irradiation. To solve this problem, a noble metal free binary photocatalyst was innovated by combining the Ta-based POM ($Na_8Ta_6O_{19}$) with the metal sulphide semiconductor ($Cd_{0.7}Zn_{0.3}S$) to synergically enhanced the stability of the composite (Zhou et al., 2019). Interestingly, the coupling of $Na_8Ta_6O_{19}$ and $Cd_{0.7}Zn_{0.3}S$ into a binary composite synergically improved the H_2-photo-evolution upon comparing to its own constituents. Upon orientated-coupling, the binary composites exhibited auspicious visible-light absorption that affirmatively augmented the solar utilization. Based on the results, the highest photocatalytic H_2-evolution (43.05% mmol/h/g) was recorded by composite with optimum $Na_8Ta_6O_{19}$ content (0.1 g). Further increasing the POM content in the composite would adversely affects the efficiency of $Na_8Ta_6O_{19}$/$Cd_{0.7}Zn_{0.3}S$ composite due to light-blocking effects arises. Furthermore, performance stability is greatly enhanced too with the same formulated photocatalyst, despite the constituents are both unstable on its own. Recyclability evaluation proves that the performance of $Na_8Ta_6O_{19}$/$Cd_{0.7}Zn_{0.3}S$ was well-maintained after four consecutive cycle of water-splitting experiment, with a minor fluctuation around 225 mmol/h/g H_2 generated in 6 h of photoreaction in all experiments.

Similar strategy was employed by Tang et al. (Tang et al., 2020) in establishing the enhanced photocatalytic performance and structural stability. Accordingly, the stability of Fe-POM was greatly improved upon bridging with TiO_2 semiconductor. Fe-POM-modified TiO_2 in this study was fabricated via two-step operation and subjected to the bisphenol-A (BPA) photodegradation evaluation. Experimentally, Fe-POM-modified TiO_2 exhibited an improved photocatalytic degradation compared to bare-TiO_2, recording almost 3-fold enhancement to 40% of BPA degradation under the same reaction conditions. The involvement of persulfate in the photoreaction further enhanced the catalytic activity, resulted from the formation of the highly reactive $SO_4^{-\bullet}$ radicals. Among the photocatalysts prepared, TiO_2 modified by 15 wt% of Fe-POM outperformed the rest, emerged as the best performed photocatalyst, exhibited the highest activity in degrading BPA (complete removal in just 20 min). In addition, the stability of photocatalyst is also closely monitored through the ICP measurements of reaction solution. Results confirmed that the Fe-content in reaction solution remained arbitrarily low, implying the suppressed dissociation of Fe-POM, hence confirming the structural stability of POM in the synthesized photocatalyst.

In addition to coupling with semiconductor material, the stability of POM can also be improved through anchoring into metal organic frameworks (MOFs). Generally, MOFs are arranged in long-range ordered topological structure with tailorable porosity, which highly beneficial in promoting the stability of POM under stringent conditions, even in tempered environment. Generally, there are four categories of POM-MOF composites:

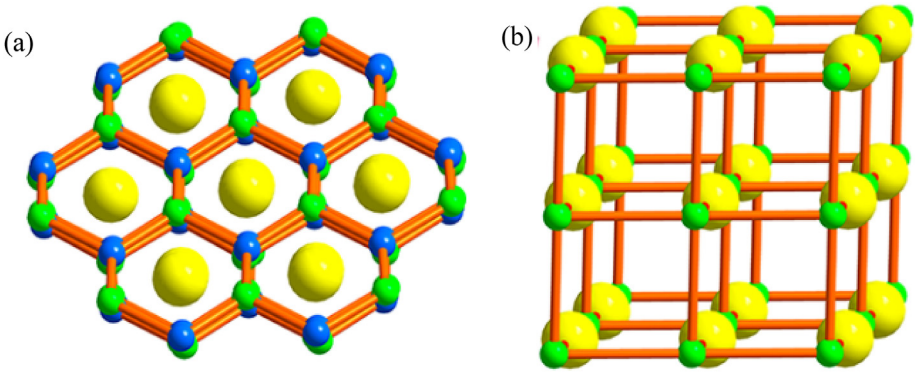

Fig. 6. Schematic diagram for (a) $[Cu^{I}_{12}(trz)_8(H_2O)_2][\alpha\text{-}SiW_{12}O_{40}]\cdot 2H_2O$ and (b) $[Cu^{I}_{12}(trz)_8Cl][\alpha\text{-}PW_{12}O_{40}]$. Reprinted with permission (Zhao et al., 2018). Copyright 2012 Elsevier.

(i) POM directively-architectured with d/f-block metal and organic units into MOF skeleton;
(ii) POM anions dwelling amid MOFs-templated framework;
(iii) spongey inorganic-organic skeleton with POM-pillars, and
(iv) POM-MOF nano-crystal composites

Despite having incredibly high stability, such structure is shadowed by its large bandgap, hence remain inactive under irradiation of low energy spectrum, especially visible light. Current speculation is confirmed by the research conducted by Wu et al. (Wu et al., 2020). The Mo-based POM-MOF was synthesized by stir-mixing $H_3PMo_{12}O_{40}$ (0.16 mmol), $AgNO_3$ (0.88 mmol), BPTD (0.05 mmol), ammonium tetramethyl hydroxide (100 μL, 1.1 mmol) in distilled water (8 mL) for 1−2 h at constant normal temperature, subsequently heated to 180 °C for three days under acidic condition (pH = 1.76), until dark blue rhomboid block crystals obtained. Evidenced from elemental analysis, the newly structured composite is given by chemical formula of $Ag_2C_{48}N_{16}H_{33}S_4PMo_{12}O_{40}$. The inclusion of S-element into the amalgamation is mainly for the widening of responsive spectrum to visible light region. As expected, the obtained binary composite of POM and MOF exhibited almost nil photocatalytic effects in decomposing RhB under irradiation of visible light even after 6 h of irradiation. To overcome this limitation, a layer of conductive polypyrrole (PPy) was deposited onto the surface of the composite, combined into a ternary photocatalyst. PPy is allegedly responsive to visible light and excel in transmitting charges, hence touted as one of the potential material in enhancing the photocatalytic effects (Tarmizi et al., 2018). Upon deposition of PPy, the activity of the ternary composite is absurdly intensified, degrading 93% of RhB under the same photoreaction conditions. It is inferred that the charges transfer processes was efficiently facilitated with PPy-coating, subsequently promoted the photocatalytic effects. In addition, the structure of ternary POM composite is also well-preserved after five cycles of photoreaction, as evidenced by both post-reaction solid XRD analysis. Furthermore, the degradation efficiencies experienced only minor depreciation, from 93.0% to 83.9% after five consecutive photoreactions in recyclability test, which however, still sufficiently high to justify the structural and performance stability.

In addition, the POM-MOF composite can also be obtained by lodging POM into the pores of pre-synthesized MOF. To synthesis this kind of POM-MOF hybrids, the frameworks structure is highly depended on the geometry, length, and coordination ability of the organic ligand. Zhao et al. (Zhao et al., 2018) constructed two distinctive but stable 3D POM-modified MOFs, *viz* $[Cu^{I}_{12}(trz)_8(H_2O)_2][\alpha\text{-}SiW_{12}O_{40}]\cdot 2H_2O$ and $[Cu^{I}_{12}(trz)_8Cl][\alpha\text{-}PW_{12}O_{40}]$, whereby Htrz is abbreviated for 1-H-1,2,4-triazole. The basic units of both POM-MOFs are $[Cu^{I}_{12}(trz)_8]$ and templated into two distinctive structures that resulted into different properties, upon the incorporation of different Polyoxoanions (POA) precursors ($[\alpha\text{-}SiW_{12}O_{40}]^{4-}$ and $[\alpha\text{-}PW_{12}O_{40}]^{3-}$). Fig. 6 shows the molecular structures of both POM-MOFs.

Structurally, the POM in $[Cu^{I}_{12}(trz)_8(H_2O)_2][\alpha\text{-}SiW_{12}O_{40}]\cdot 2H_2O$ was embedded in the nanopores of the MOF frameworks, while for $[Cu^{I}_{12}(trz)_8Cl][\alpha\text{-}PW_{12}O_{40}]$, the POM acted as building unit and ionically bonded to the MOF. Subsequently, both photocatalysts were subjected to RhB degradation under irradiation of visible light and attaining superior degradations, 91% and 81% for $[Cu^{I}_{12}(trz)_8(H_2O)_2][\alpha\text{-}SiW_{12}O_{40}]\cdot 2H_2O$ and $[Cu^{I}_{12}(trz)_8Cl][\alpha\text{-}PW_{12}O_{40}]$ respectively. These enhanced photocatalytic effects are mainly attributed to the coefficient effects exhibited by the POMs and MOFs. The amalgamation of MOF units in the composite further facilitate the charges transfer upon photoexcitation, hence enhances the photocatalytic effects. In addition, the high stability of $[Cu^{I}_{12}(trz)_8(H_2O)_2][\alpha\text{-}SiW_{12}O_{40}]\cdot 2H_2O$ was also confirmed through the recyclability test, whereby no obvious activity loss after 5 cycles of RhB degradation. Structural prevails was excellently preserved too as confirmed by post reaction XRD analysis. Such high performance and structural stabilities are mainly derived from the superior 3D frameworks that encapsulating the reduced POMs, hence stabilizing it via rapid re-oxidization process by donating electrons to the dissolved oxygen. Current findings in stabilizing POM-MOF composites are also well accepted and further confirmed by other literatures (Li et al., 2018; Zhao et al., 2018). In addition, the recent advances of POM-MOF composites, including the design strategies and potential applications are well summarized in review published by Li and group (Li et al., 2019).

In addition to performance and structural stabilities, the recoverability of photocatalysts is also crucial for the consideration of practicality. Generally, synthesis of nano-sized POM photocatalysts is highly favorable for its large reactive surface, which however deriving into another huge challenge of recovery difficulties. Conventional recovering techniques employed are prolonged vacuum filtration and centrifugal separation that accompanied with intensive energy requirements, hence leading to impracticality of nano-photocatalysis. To solve this problem, immobilization of nano-sized POM photocatalysts onto a larger supports grain could be one of the effective ways in advocating facile separation. Among the supports, SiO_2 is commonly employed (Guo et al., 2000; Kumar & Landry, 2007; Yue et al., 2002), owing to its high surface area, outstanding optical properties and highly tunable structures. For instance, Guo et al. (2000) synthesized microporous silica-immobilized POM photocatalysts by evenly dispersing $H_3PW_{12}O_{40}$ and $H_4SiW_{12}O_{40}$ into silica bulk phase, separately, through sol-gel technique. As results, two set of POMs/SiO_2 photocatalysts were successfully obtained and exhibited

improved properties, such as high insolubility (structural stability) and readily separable behaviour. Furthermore, the photocatalysts were also complimented by high specific surface areas adopted from the microporous structure of SiO_2 support. Based on the results, both microporous silica-supported POM photocatalysts yielded considerable of hexachlorocyclohexane removal (*circa* 50% both cases), synchronously featured with enhanced practicality from the photocatalyst recovery prospect. It is claimed that photocatalyst is readily to be separated by only gravitational sedimentation. Similar finding was also reported by Yue et al. (2002). A series of silica-immobilized POM photocatalysts were prepared by using different POM-precursors, *viz* $Na_6W_7O_{24}$, $H_4W_{10}O_{32}$, $H_3PW_{12}O_{40}$, and $H_6P_2W_{18}O_6$, via sol-gel method. By comparing with their corresponded bare POM, all the immobilized POM photocatalysts manifested promoted photocatalytic effects in degrading 4-chlorophenol upon the inclusion of SiO_2 support. It is reported that the advantageous large area-to-weight ratio of SiO_2 facilitated the chemisorption of the substrate, hence accelerated the photocatalytic degradation process. Similar with previous study, the separation of all the photocatalysts was performed by energy-free gravitational sedimentation and satisfactory separation could achieved in just 30 min.

In addition to separation convenience, immobilization of nano-POM photocatalysts onto larger support can effectively prevent the agglomeration of photocatalyst, hence maximizing the utilization rate of active surfaces. The strategies in constructing such morphology were critically summarized and reviewed from the perspectives of solid support selections, metallic precursors selections, as well as interaction between supports and dispersed particles by Zhao and co-workers (Zhao et al., 2018). In addition, prevention of POM leaching from the support is also vital in maintaining the performance consistency. To hinder the leaching of POM, an ingenious immobilization method were proposed by Kumar & Landry (2007), which encompassing chemical interactions between Silica-support and POM-photocatalyst. Based on the report, MCM-41 silica support was cationically-modified, subsequently mixed with anionic $PV_2Mo_{10}O_{40}^{5-}$ for the ionic interactions. FTIR of resulting solid indicates the newly emerged band at 870 cm^{-1} and blue-shifting of POM bands upon modification, hence evidences chemical bonding between POM and MCM-41 silica support. Such chemically-bounded structure effectively retains POM on the surface of MCM-41 silica, at the same time promotes the transfer of photo-generated charges.

In addition to immobilization, the recovery of photocatalysts can be assisted by magnetic separation too. Generally, magnetite properties can be fostered into POM photocatalyst via engraftment of magnetic component, particularly Fe-based constituent. For instance, TiO_2/FeO_x/POM photocatalyst was prepared by using W-based POM ($Na_3[PW_{18}O_{40}]$) to accelerate the photocatalytic removal of 2,4-dichlorophenol, at the same time cater the photocatalyst recovery after photoreaction (Yu et al., 2019). As opposed to bare-TiO_2, incorporation of 25 wt% of FeO_x with NH_3-assisted deposition widens the light absorption spectrum to visible-light region, thereby enhancing the photocatalytic activity of TiO_2/FeO_x under solar light irradiation. Whilst, the doping of 1 wt% of POM onto bare TiO_2 improved the absorption of UV spectrum and stimulated the shuttling of photo-excited electron, hence significantly enhanced the photodegradation of 2,4-dichlorophenol to 87.5% with 6 h of photoreaction. However, upon including both FeO_x and POM (25 and 1 wt% respectively) onto TiO_2, a relatively lower efficiency of 76.0% of 2,4-dichlorophenol removal was recorded, as a trade-off for photocatalysis recovery convenience. The slight hindrance observed herein could be ascribed to the blockage of active sites on the surface of TiO_2 photocatalyst upon the deposition of POM. In addition, other potential risk such as leaching of Fe-content from photocatalyst upon photon irradiations could also lead to the activity loss and regarded as secondary pollution (Ding et al., 2012; Feng et al., 2006; Liang et al., 2017). Reasonably, Fe-content in photocatalysts is highly susceptible to reduction by excited-electron, subsequently photo-dissociates in substrate solution during photoreaction. Fortunately, these issues are readily solved via the preparation of core-shell structures (Qiu et al., 2007; Shi et al., 2006). Shi et al. (Shi et al., 2006) synthesized the magnetical POM-photocatalyst via progressively coating method, initiate with the magnetite Fe_3O_4 core, subsequently coated with Ag and $PW_{12}O_{40}$-POM layer in sequence. By comparing with bare POM, the double-layer-coated photocatalyst exhibited enhanced photocatalytic degradation ability towards RhB when irradiated by visible light. This is mainly resulted from the chemically-linked of the shell layers and magnetite Fe-core that facilitates the charges separations. In addition, ICP analysis of post-reaction substrate solution reveals that such core-shell structures sharply reduced the photo-dissolution of Fe-metal by eliminating the direct contact of Fe-core with water substrate. Other methods, *viz* photo/electrochemical-thermal method (Castañeda-Juáreza et al., 2019), integration of Fe-material into the support's skeleton (Hu et al., 2019) and complexation with chitosan (Zhao et al., 2020) are also investigated and proven effectively preventing the leaching Fe-content from the catalyst matrix. Despite not applying upon POM, all these past researches still provide provisional guidelines and strategies in retaining both structural stability and magnetic properties in the POM photocatalyst.

As a summary, current section reviewed and summarized some of the critical endeavors in improving the practicality of POM photocatalysis. As mentioned, the practicality of POM-photocatalysts is highly suppressed by its highly dissociative tendency, hence leading to inferior performance and structural stability. In addition, recoverability of POM-photocatalyst also plays a crucial role in ensuring the reusability and hence its practicality in photocatalysis. Therefore, current section provides insightful strategies in improving abovementioned aspects. As summary, the practicality of POM photocatalysis can be enhanced from the following perspectives:

1. By improving the photocatalytic performance in degrading organic pollutants. The performance of Keggin-based POM photocatalyst can be enhanced by incorporation of optimum amount impurities (either dopants, photocatalytic-supports or co-catalysts). When acted as dopant, the typical optimum amount of Keggin-based POM-dopant would be under 20 wt% for the best photocatalytic activity. Upon taken as photocatalytic support, the inclusion of dopants might induce enhanced photocatalytic effects, typically with optimum amount under 20 wt % too. As for co-catalyst, the ratio of Keggin-based POM for optimum photocatalytic performance could be varied according to different materials and hence detailed investigation is needed.
2. By improving the structural stability. Fortunately, due to its highly tailorable molecular structure and properties, the dissociative tendency can be greatly alleviated via different methods, including coupling with other semiconductors, complexation of POM-material, inclusion of MOF and others.
3. By improving the recoverability. The recoverability can be improved via the immobilization of Keggin-based POM nano-photocatalyst onto the surface of larger particle. However, effective synthesis methods are required to impede the potential leaching issues. In addition, magnetic separation would be another effective recovery approach, provided that photocatalyst must be magnetized in advanced.

3.2. Process intensification of Keggin-based polyoxometalate photocatalysis

In addition to modification of Keggin-based POM photocatalyst, the design of experiments such as the operating catalyst loading, initial concentration of substrate and pH are commonly investigated for the establishment of enhanced photocatalytic effects and hence, the practicality of the Keggin-based POM photocatalytic system. Current section summarizes the findings from the past researches herein (Du et al., 2019; Hu and Xu, 2004; Li et al., 2019; Lu et al., 2017; Mahmoodi et al., 2016; Meng et al., 2019; Qiu et al., 2007; Rafiee et al., 2020; Shahrnoya et al., 2018; Zhao et al., 2013), focusing on the effects of each operating parameter mentioned above.

3.2.1. Initial concentration of substrates

Generally, substrate's initial concentration is as of importance in determining the overall photocatalytic efficiency of Keggin-based POM photocatalyst. It is suggested that the initial concentration of substrate contributes a positive effect to photocatalytic system up to an optimum point only. Indeed, the concentration of substrate is closely related to the utilization rate of the photo-active sites of photocatalysts. The increment in initial concentration will theoretically facilitate the mass transfer of substrate across the liquid-solid boundary, promote adsorption of substrate onto the active sites, hence enhance the degradation rate resulted from the higher coverage rate of the surface. This is particularly true when the photocatalytic system is free from mass transfer limitations. Evidently, most of the organic photo-degradation reactions adhere to first order reaction kinetic (Cheng et al., 2016; Ng and Cheng, 2015, 2016; 2017; Ng et al., 2016a, 2016b; Ng et al., 2019), in which increase in concentration leading to the enhanced degradation rate. However, beyond the optimum point, further increasing the concentration of substrate will lead to an adverse effect onto the photocatalytic activity. Summarizing the past researches, this phenomenon could be ascribed to:

1. Saturation of active sites. In the presence of excessive substrate, the saturation of active sites on photocatalyst's surface is possibly encountered. The degradation, therefore, is limited by the intrinsic kinetic of the photocatalyst and insensitive towards the increment of substrate concentration.
2. The adsorption competition with the intermediate products. Generally, the substrate, particularly big molecule organic pollutant, will be subjected to decomposition into smaller intermediates prior to the total photo-mineralization. This elicited the adsorption competition between these intermediate fragments with the main substrate on the surface of POM-based photocatalyst, particularly at high concentration; ergo, an adverse effect is observed.
3. The induced light-scattering effects. Light scattering effects, sourced from the refractory organic pollutants or dyes, are widely impeached for the declining degradation trend at high concentration. With the limited light penetration into substrate solution, the activity of suspended POM-based photocatalysts was reduced synchronously due to scarcity of driving force, therefore leading to poor photo-degradation efficiency.

3.2.2. Operating photocatalyst loadings

The operating POM photocatalyst loading also exhibits a similar trend in the photo-degradation of organic pollutants, whereby an optimum point will be observed and separated the degradation efficiencies into two distinctive regions. Theoretically, before the optimum point, enhanced photocatalytic activity will be observed with increment of POM photocatalyst loadings due to the increased reactive surface. Furthermore, by increasing the POM photocatalyst loading, the degradation mean free path between the reactive species, for instance the OH• free radical, with the substrate (Ng et al., 2017). However, as the loading increase beyond optimum point, the adverse effects would be aroused from the following reasons:

1. The increased opacity of the substrate solution resulted from the suspension of high dosage POM photocatalyst. The penetration of light into the suspension will be greatly reduced hence leading to the suppressed photocatalytic activity.
2. The agglomeration of POM photocatalyst. With excess POM photocatalyst, there is high tendency of agglomeration occurrence, particularly for those that designed with high-energy surfaces, to attain lower overall energy position for stabilizing purpose. Losses of reactive surface from agglomeration would also contribute to the reduced photocatalytic activity observed.

3.2.3. pH changes

Unlike the above mentioned two operating parameters, the photocatalytic activity doesn't manifest an obvious general trend with respect to pH changes. Therefore, it is worth to summarize the detailed and critical findings on effects of initial pH of substrates towards the photocatalytic activity. Based on Qiu et al. (2007), acidic environment is preferred for the formation and preservation of OH• radical, hence inducing an enhanced photodegradation of organic components. Accordingly, 1.6-fold of improvement was discovered as the initial pH was lowered from 3.5 to 1.0 while maintaining the other reaction conditions over $H_3PW_{12}O_{40}$-based photocatalysis. This finding is also agreed by Hu & Xu (Hu and Xu, 2004). The research team investigated photodegradation of textile dye X3B by several POM photocatalysts, including bare $H_3PW_{12}O_{40}$. Results reveal that the apparent reaction constant, k_{app}, for $H_3PW_{12}O_{40}$ significantly reduces from 1.14×10^{-2} min^{-1} to 5.29×10^{-3} min^{-1} when the pH increases from 1.0 to 3.0. Such declining activity could be correlated to the structural changes of PW_{12} to PW_{11} in POM resulted from pH increment. This is totally reasonable, considering POM is highly sensitive to pH change and susceptible to hydrolysis as pH increases. Keggin POM-based acid compound, such as $H_3PW_{12}O_{40}$ mentioned, will progressively lost metal-oxide octahedron (MO_6) entities from its structure as pH arises, forming the Lacunary compound (Cavani, 1998). A further confirmation was also obtained from the past research herein (Yang et al., 2012).

However, wastewater containing organic pollutants does not always come in low pH in real world. Chemically altering pH prior to the photocatalytic treatment could be effective mean to preserve the stability and catalytic performance, which however economically infeasible and potentially causing secondary pollution. Fortunately, this issue can be readily solved via incorporation of MOF or compositing with semiconductor, as presented in previous sub-section. It is worth mentioning that a composite photocatalyst (PW_{12}@MFM-200(In)) were isolated from the solvent-free hot-pressing of $H_3PW_{12}O_{40}$, $In(NO_3)_3$ and Biphenyl-3,3′,5,5′-tetracarboxylic acid into the POM-MOF hybrids (Li et al., 2019). Such rapid and facile method successfully immobilized the POM material into the pores of MOF by solely physical imprisonment, at the same time renders it with relatively higher pH resilience indicated from the high recyclability test. The photo-degradation of PhAC sulfamethazine (SMT) also evidences that such modification opens up the pH-activity of PW_{12}@MFM-200(In) photocatalyst, recording a considerable activity from pH 2.0–8.0, with optimal point located at pH 6.0 (>90%). At pH 6.0, adsorption of SMT was electrostatically

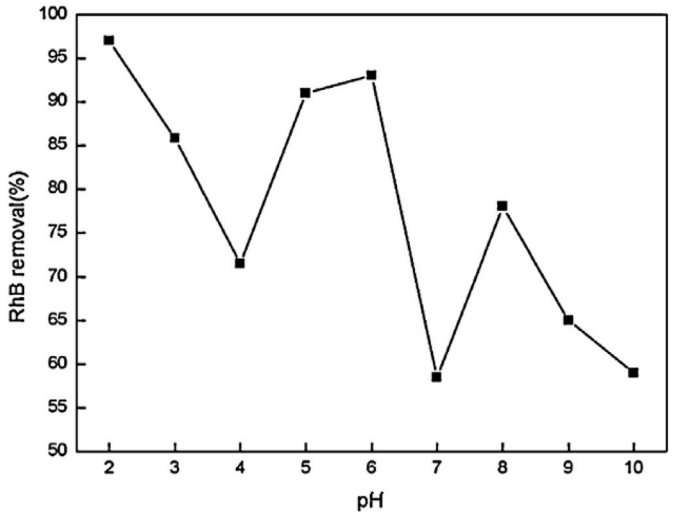

Fig. 7. The adsorption study of RhB on $[Ni(bipy)_2]_2(HPW_{12}O_{40})]$ powder over different pH, Initial concentration of RhB: 25 ppm; POM-powder concentration: 0.01 g/L; Temperature: 25 °C Reprinted with permission (Li et al., 2015). Copyright 2015 Elsevier.

facilitated by pH-induced charges on the surface of PW_{12}@MFM-200(In) (with reference to the pH for point-of-zero-charge, $pH_{pzc} = 5.8$). In addition, the authors also revealed that an undesired electrostatic repulsion force will be established in between SMT molecules and photocatalyst at pH out of 2.28−7.42, which explained the relatively lower photodegradation efficiency observed at pH = 8.0.

Such facilitation/inhibition of substrate adsorption theory is further confirmed by Lu et al. (2017). POM-based photocatalyst was prepared by depositing 10 wt% $H_3PW_{12}O_{40}$ onto TiO_2 film in the presence of 1 wt% of Ag. Similarly, this formulated POM-based photocatalyst exhibited an optimum stability and performance activity at a relatively neutral condition for the photo-degradation of *ortho*-chlorophenol (*o*-CP) under irradiation of simulated solar light. Specifically, 82.40% of *o*-CP degradation was observed at pH = 6.3 compared to 46.80% at pH = 3.1, 73.80% at pH = 12.1 and 79.70% at pH = 9.2. The dark experiment suggested that the superior degradation observed at pH = 6.3 is largely attributed to the synergetic effects from the high adsorption rate and pronounced degradation tendency of *o*-CP at high pH. Theoretically, an acidic environment would stimulate the positive-charged photocatalyst surface, which promote the attachment of negatively charged *o*-CP to it. However, under the extremely acidic environment (pH = 3.1), the excess H^+ will be bonded to both photocatalyst surface and *o*-CP molecule, subsequently plummeting the adsorption phenomenon due to electrostatic repulsion forces. Therefore, the adsorption of *o*-CP molecules is favorable at mild acidic (pH = 6.3) environment as shown (Lu et al., 2017). These results obtained marked that pH is highly significant, not only in affecting the stability of POM photocatalyst and adsorption phenomenon, but also in interacting with the pollutants for a more unassuming photo-degradation.

In addition, the interaction between pH and organic pollutant would also lead to the different degree of distorted adsorption process. One of the good example is the RhB adsorption study on the $[Ni(bipy)_2]_2(HPW_{12}O_{40})]$ powder conducted by Li et al.(Li et al., 2015). The results obtained are adopted and portrayed in Fig. 7.

As indicated in Fig. 7, the adsorptive behavior of RhB fluctuated interestingly across pH 2.0−10.0, correspondingly implied the adsorption capacity of $[Ni(bipy)_2]_2(HPW_{12}O_{40})]$ powder under acidic/alkaline environment. This may attribute to the interaction of pH with the surface of POM powder and/or the ionizative/dissociative tendencies of molecules. It is unsurprising that different pH environment can induced several impacts to the system, including pH-stimulated surface charges of powder, ionization condition of adsorbate molecule and magnitude of dissociation of functional groups on the active sites of adsorbent (Nandi et al., 2009). Technically, RhB is an amphoteric component with both amino group ($-NHR_2$) and carboxyl group (-COOH) covalently-bonded in the chemical structure. At extremely acidic condition (pH = 2.0), RhB is more prone to cationic and monomeric that sufficiently small in size for the adsorption onto internal surface within the pores. As the pH increased to 4.0, the absorption of RhB hits the first low point, mainly due to the reduced monomeric characteristic (bigger in size thus being has no accessibility across the small opening pores) and the steric hindrance resulted from the pH-induced charges. As pH increased further to a relatively neutral environment (pH = 6.0), an increasing spike of RhB adsorption was re-emerged due to the progressively-relieved electrostatic repulsion forces between RhB positive ion and cationic $[Ni(bipy)_2]_2(HPW_{12}O_{40})]$ powder. Subsequently, an absurd decrease in RhB absorption to minimum point (~57.0%) was observed, possibly resulted from bulky molecule formation due to the dimerization of RhB zwitterions (Deshpande & Kumar, 2002). As more OH^- being introduced (pH = 8.0), it will be electrostatically attracted to the $-N^+$ in the zwitterion of RhB, thereby inhibited the dimerization while preserving its tininess and susceptible to pores diffusion. Unfortunately, further increasing the OH^- leads to the undesirable electrostatic repulsion between RhB and $[Ni(bipy)_2]_2(HPW_{12}O_{40})]$ powder, hence the decreased absorption rate was observed in Fig. 7.

The adsorptive study presented above portrayed the importance of pH interactions, whether with molecule or the adsorptive surface, in affecting the absorption behavior, as well as the photo-degradation of substrate molecules over a POM photocatalyst. However, the optimum pH indicated herein is only provided as a guideline and might not representable for all systems with different POM photocatalyst or different targeted substrate. A detailed experimental investigation is still required for more authenticable data.

3.2.4. Boosting agents

Some researchers opted to enhanced the overall photocatalytic efficiency via the addition of boosting agent, commonly H_2O_2, cited herein (Antonaraki et al., 2002; Luo et al., 2016; Wang et al., 2013; Yang et al., 2012; Zhai et al., 2016). It is touted that H_2O_2 is added to promote the formation of OH• radical via the activation of photo-excited electrons or homolytical splitting under irradiation of UV light (<370 nm) (Antonaraki et al., 2002). In addition, for Fe-containing POM photocatalyst, photo-fenton-like process would also be triggered thereby forming more OH• radical (Zhai et al., 2016). These OH• radicals are highly unselective and reactive that complete mineralization of organic pollutants is even possible under the optimized conditions. However, the added H_2O_2 will be consumed in exchange of the enhanced photocatalytic effect and successive additions, hence higher cost, are required to maintain the satisfactory performance. Whether such operation is compensable from the perspectives of economic feasibility and practicality, we leave it as an open question to the researchers and advancement of future technologies.

Concluding for current section, the process intensification is indeed very important in enhancing the practicality of Keggin-based POM photocatalysis. Commonly investigated operating factors, such as initial concentration of substrate, POM photocatalyst loading, operating pH and addition of performance booster (H_2O_2) are significant in affecting the photocatalytic activity. Apparently, the agglomeration of Keggin-based POM photocatalyst particle can be electrostatically controlled by pH, hence possibly exhibiting an

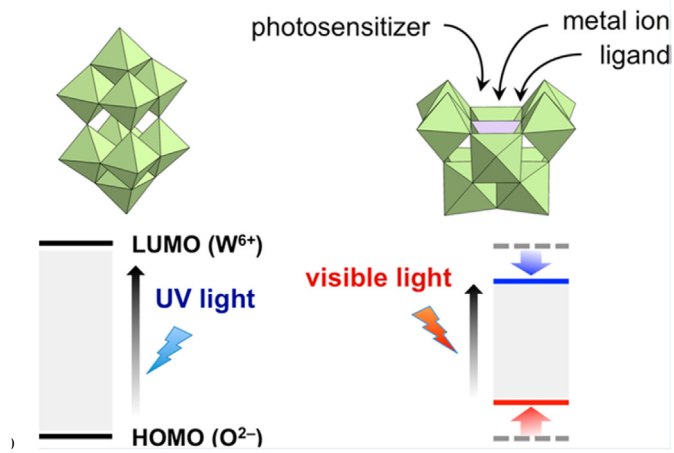

Fig. 8. UV responsive through charge transfer from the O_2^--based HOMOs and the W^{6+}-based LUMOs. Visible lights responsive POM catalysts through hybridization with photosensitizer, metal substitution, and introduction of ligands (substrates) at the vacant sites of lacunary POMs. Reprinted with permission from (Suzuki et al., 2018). Copyright 2018 American Chemical Society.

entirely different optical property. Likewise, the stability of substrate would also be affected by the pH, depending on the reactivity and sensitivity of it, and so forth. Therefore, the interactions among the factors are worth for examination and employment of the established optimization techniques, such as Box-Behnken or Central Composite Design in the Design Expert software, are highly recommended for adequate and comprehensive statistical evaluation.

4. Fundamentals of Keggin-based polyoxometalate photocatalysis

After reviewing synthetic methods and intensified processes of the nanocomposites, this section will discuss about the working principles, encompassing photochemistry and mechanisms. The binary and ternary structures of Keggin-based POM nanocomposites will be illustrated.

4.1. Photochemistry

Similar with other photocatalysts, POMs require the irradiation of light with equals or greater than its bandgap for photoexcitation. The photo-induced POM nanocomposites experience electron excitation from ground state (valence band) to excited state (conduction band). In details, the electrons excited are originated from oxygen atoms within POM nanocomposites, which is accustomed to as a group of metal-oxo nanoclusters (Streb et al., 2019; Suzuki et al., 2018). Then, the excited electrons jump to the conduction band, which attributing to *d*-orbitals of early transition metals with high oxidation states. For instance, O_2^--based highest occupied molecular orbital (HOMO) to *d*-orbital of W^{6+}-based lowest unoccupied molecular orbital (LUMO) in the POM framework. This process generates electron-hole pairs that turn photoexcited POM into oxidizing agent (holes) and reducing agent (photogerated electrons on the surface) for the subsequent reactions (Suzuki et al., 2018). The excited electrons on the conduction band could photochemically reduce oxygen to produce superoxides, $\bullet O_2^-$ anions. Subsequently, the superoxides attack water molecules, hydroxyl radicals, OH•, are generated. The positive holes generated by photoexcited electrons, also generate OH• radicals after interacting with water molecules (Chiu et al., 2019; Nikoonahad et al., 2018; Streb et al., 2019). Those radicals are exceptionally effective in degrading the recalcitrant pollutants in water bodies.

For visualization purpose, Kosuke Suzuki and co-researchers (Suzuki et al., 2018) have illustrated the working principle for POMs upon irradiation of different light sources (refer Fig. 8). For POMs which respond to UV irradiation, metal-oxo clusters bearing early transition metals, such as tungsten (W) has high oxidation state, resulting in d^0 electronic configuration upon oxidation; thus, it has empty orbitals to accept electrons excited from O^{2-}. This has demonstrated ligand-to-metal charge transfer (LMCT) phenomenon, under illumination of UV light. Nonetheless, due to this wide energy bandgap concern, many literature reports have intensively focused on narrowing down the bandgap (Streb et al., 2019; Suzuki et al., 2018) by structure modification so that POMs could respond to longer wavelength (visible region) with lower energy absorption. One of the enhancement method is to remove one or more addenda metals in POMs, together with their shared oxygen atoms, therefore creating the defective, vacant sites in POMs structure. This defected-structure is named as Lacunary structures (depicted in Fig. 8), and is highly reactive and susceptible to modification via photosensitization, metals substitution and ligands hybridization due to the presence of vacant sites. Visible light-sensitive materials could be incorporated to extend the light absorbability of POMs, hence reducing the band gap energy of the composite material.

Notwithstanding POM nanocomposites carry out the similar mechanisms as other photocatalysts, POM nanocomposites surpass others with their exceptionally structural stability during photooxidation-photoreduction. The empty orbitals of metal ions can transport electrons back and forth a variety of organic pollutants. The oxidized oxygen (loss of electrons to conduction band) can regain the electrons from H_2O surrounding. More interestingly, adding different rations of metal ions into the POM framework could tune the band positions at the molecular level, to degrade a range of unknown recalcitrant pollutants. This is particularly important in tuning the redox potentials, and hence their oxidation and reduction abilities according to the applications, particularly in diversifying its photocatalytic effects. In addition, POMs can accommodate multiple electrons due to the prevailing electronics structure, allow the promotion of multi-electron redox reactions that facilitates the conversion of sunlight into chemical energy (Streb et al., 2019; Suzuki et al., 2018).

4.2. Photo-mechanisms

Based on past research works, it can be surmise that POM-based photocatalysis exhibited different mechanisms under different structural configurations. Typically, it is categorized into three types, *viz* bare POM, POM-based binary and ternary nanocomposites. Notably, the mechanism of bare POM has been presented in Section 4.1. For the POM-based binary and ternary nanocomposites, the mechanisms are presented in the following sections to provide an insightful fundamental understanding, particularly to new researchers.

4.2.1. Binary of POM/semiconductor

In a binary photocatalyst, POM is mainly incorporated as doping agent and inserted into the interstitial of another species of semiconductor. Thus, this creates a new electronic state in between the valence and conduction bands of semiconductor, resulted to a POM composite with lower E_g. Furthermore, with proper preparation methods, the chemical interactions between POM and other materials can be established. For an instance, photodegradation performance of Crystal Violet over pristine Keggin-based POM was 79.7% in 36 min (2.21 min^{-1}), however, it surged up to 94.3% in

36 min (2.62 min^{-1}) upon incorporated with MOF consisted of electron acceptor and shuttler, *i.e.* TTPB-4 or 1,3,5-tris(4-(4H-1,2,4-triazol-4-yl)phenyl)benzene] (Liu et al., 2018). TTPB-4 could accept the excited electron from conduction band of POM and transfer it to adsorbed O_2 to form superoxide, $\bullet O_2^-$. In addition, it is worth noting that the intrinsic, individual Ru(II) bis(terpyridine) photosensitizer has a considerably short excited-state lifetime, in the range of 124–250 ps, which varying with the solvents used. However, the charge-separated state or excited-state lifetime was enhanced to long-lived one, *ca.* 470 ns, detected by ns transient absorption spectroscopy. This infers that the interaction between a photosensitizer, Ru(II) bis(terpyridine) and Keggin-based POM, $[PW_{11}O_{39}Ge]^{4-}$, could prolong the lifetime of the photo-populated charge-separated states (CSS), to attack substrates or pollutants surrounding it (Luo et al., 2018). Besides, the photoinduced electron with longer lifetime could expedite its movement to the surface of POM, due to its high electron storing ability, thus this can prevent a fast electron/hole reintegration (Nikoonahad et al., 2018).

Taking W- or Mo-based POM photocatalyst as model component (Nikoonahad et al., 2018), the photogenerated electron (e^-) at the semiconductor after photons striking (Equation (1)), will be cascaded into a vacated W_{5d} or Mo_{5d} state, to form POM^- (Equation (2)). Given its reducing ability, the POM^- can transfer the photo-excited electrons to adsorbed O_2, causing the O_2 generates superoxides, $\bullet O_2^-$ (Equation (3)). POM^- hastens the transportation of electron from the semiconductor to O_2 and simultaneously obstructs the electron-hole pairs reintegration (Nikoonahad et al., 2018). The $\bullet O_2^-$ produced possesses certain degree of activity, with portion of it scavenged by water molecule according to Equation (4), subsequently forming $\bullet OH$ for degradation of organic pollutants. The remaining $\bullet O_2^-$ is consumed by the direct oxidation of organic pollutant in accordance to Equation (5) to attain the degradation process. The photoinduced holes on the semiconductor are unavoidably interact with water molecules or OH^-, yielding highly reactive $\bullet OH$ for organic pollutant degradation after a series of reactions (Equations (6)–(9)).

$$\text{Semiconductor} \xrightarrow{h\nu} \text{Semiconductor}(h^+ + e^-) \quad (1)$$

$$\text{Semiconductor}(e^-) + \text{POM} \rightarrow \text{Semiconductor} + \text{POM}^- \quad (2)$$

$$\text{POM}^- + O_2 \longrightarrow \text{POM} + \bullet O_2^- \quad (3)$$

$$\bullet O_2^- + H_2O \longrightarrow \bullet OH + OH^- \quad (4)$$

$$\bullet O_2^- + \text{Organic pollutants} \xrightarrow{[O]} \text{Degraded products} \quad (5)$$

$$\text{Semiconductor}\ (h^+) + H_2O \longrightarrow \text{Semiconductor} + \bullet OH + H^+ \quad (6)$$

$$\text{Semiconductor}\ (h^+) + OH^- \longrightarrow \text{Semiconductor} + \bullet OH \quad (7)$$

$$\text{Semiconductors}(h^+) + \text{Organic pollutants} \xrightarrow{[O]} \text{Semiconductors} + \text{degraded products} \quad (8)$$

$$\bullet OH + \text{Organic pollutants} \xrightarrow{[O]} \text{Degraded products} \quad (9)$$

In addition to electron-acceptor as abovementioned, POM can also functionalized as photocatalyst upon appropriate light-activation. In consequence, excitation of electrons from ground

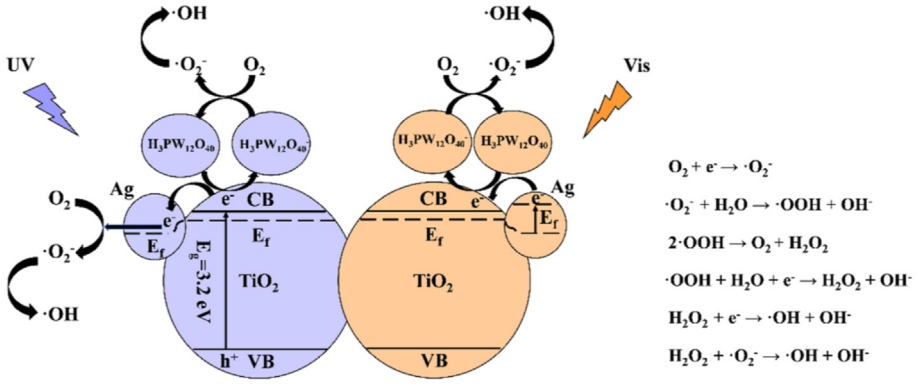

Fig. 9. The photocatalytic mechanism of Ag-TiO_2/$H_3PW_{12}O_{40}$ system. Reprinted with permission from (Lu et al., 2017). Copyright 2017 Nature Publishing Group.

state of Keggin-based POM-semiconductor nanocomposite also prompts to occur. By taking the same W- or Mo-based Keggin POM again, upon excitation, an electron will be generated from POM, resulting to the charging transfer from O^{2-} to W^{6+} or Mo^{6+} (in W-O-W or Mo-O-Mo, respectively), forming W^{5+} or Mo^{5+} ion (Equation (10)). The reduction of metals (W or Mo) in POMs effectively trapped the photogenerated electron, at the same time forming a O^- ion in POM structure (Equation (10)) (Nikoonahad et al., 2018).

This mentioned O^- ion exhibited a strong oxidation ability, which is responsible for oxidizing pollutants by accepting an electron. The water molecule and organic pollutants are competitively adsorbed onto POM positive holes, thus giving electrons to the holes and themselves get oxidized to form •OH, H^+ and degraded products (Equations (11) and (13)). The •OH radicals degrade those surrounding organic pollutants spontaneously (Equation (12)). On the other hand, superficial electrons on POM^- react with O_2 to form superoxide radicals, $\bullet O_2^-$ (Equation (14)). In the subsequent step (Equation (15)), $\bullet O_2^-$ radicals are actively in degrading those organic pollutants collide with them, hence the pollutants are mineralized or degraded.

$$\left[W^{6+} - O^{2-} - W^{6+}\right] \xrightarrow{h\nu} \left[W^{5+} - O^{-} - W^{6+}\right]^{*} \text{ or } POM^{*} \quad (10)$$

$$POM^{*} + H_2O \longrightarrow POM^{-} + \bullet OH + H^{+} \quad (11)$$

$$\bullet OH + \text{Organic pollutants} \xrightarrow{[O]} \text{Degraded products} \quad (12)$$

$$POM^{*} + \text{Organic pollutants} \xrightarrow{[O]} \text{Degraded products} \quad (13)$$

$$POM^{-} + O_2 \longrightarrow POM + \bullet O_2^{-} \quad (14)$$

$$\bullet O_2^{-} + \text{Organic pollutants} \xrightarrow{[O]} \text{Degraded products} \quad (15)$$

Summarizing from aforementioned reactions, in binary photocatalyst, both POM and semiconductor constituents are effective in generating reactive species for organic pollutants degradation upon photo-excitation via appropriate light-irradiation. Furthermore, with proper preparation methods, the chemical interaction between them could be established, facilitating the transfer of photogenerated electron, hence synergically enhanced the photocatalytic reactivity.

4.2.2. Binary structure of POM/polymer sensitized by H_2O_2

Photocatalysis is well-known for its versatility and effectiveness towards organic pollutants, including large and stable organic pollutants. However, for these recalcitrant organic pollutants, photo-degradation process could be attributed to two major pathways:

(i) the common photo-excitation of photocatalyst, subsequently, generation of hydroxyl radical for photo-mineralization process, as presented in Section 4.2.1; and
(ii) the photoexcitation of large and recalcitrant organic pollutants, followed by redox reaction of POM-based nanocomposites

Current section focuses on the latter pathway, with particular emphasize given to binary POM-based nanocomposites. Generally, upon photo-excitation of substrate or recalcitrant organic pollutants, an electron will be discharged from pollutant and accepted by POM, owing to its excellent electron storing ability. The acceptance of the electron induces a negatively-charged POM initially, then undergoes a complexation process with the present oxidants, *i.e.* O_2 and H_2O_2, forming a very reactive peroxo-complex towards the destruction of organic pollutants.

For instance, Lei and co-workers (Lei et al., 2005) prepared a binary photocatalyst by immobilizing W-based Keggin-POM/resin ($PW_{12}O_{40}^{3-}$) on an anionic polymer, *i.e.* resin, through electrostatic interaction for Rhodamine B (RB) photo-degradation. Based on the mechanisms illustrated in equations 16–19, the pre-association between cationic RB and W-based Keggin-POM/resin is required to facilitate the transfer of electrons (equation (16)). The ingenious selection of anionic resin as support further promoted the association of RB and POM/resin due to the charges interactions. Under visible light irradiation, the excited electrons from RB accumulate high energy and display high electron density at their region, then they migrate to the lowest unoccupied molecular orbital (LUMO) of the POM (equation (17)). As a consequence, a reduced POM/resin and oxidized $RB^{+\bullet}$ radical pair can be generated from the electron-transfer process.

The reduced POM/resin are susceptible to complexation process, then they are slowly re-oxidized to $PW_{11}O_{39}^{7-}$/resin in the presence of O_2 and co-produced •OOH radicals adsorbed on the POM, hence causing de-ethylation of RB (equation (18)). To further enhance the process, H_2O_2-oxidant can be used under acidic conditions to ramp up the complexation process, subsequently forming the coordinated W-O peroxo species (equation (19)). Subsequently, the obtained peroxo species exhibited high activity and chemically interact with the $RB^{+\bullet}$ radicals, resulted to the photocatalytic degradation of the RB dye (Lei et al., 2005).

$$RB + POM/resin \rightarrow [RB - POM/resin] \quad (16)$$

$$[RB\text{–}POM/resin] \xrightarrow{h\nu} [RB^{*}\text{–}POM/resin] \longrightarrow [RB^{+\bullet}\text{–}POM^{-}/resin] \quad (17)$$

$$[RB^{+\bullet}\text{–}POM^{-}/resin] \xrightarrow{O_2,\ H^+} [RB^{+\bullet}\text{---}POMOOH/resin] \longrightarrow \text{De-ethylated products} \quad (18)$$

$$[RB^{+\bullet}\text{–}POM^{-}/resin] \xrightarrow{H_2O_2} \left[RB^{+\bullet}\text{-----}O\text{-}O^{-}\text{-}W\text{-}/resin\right] \xrightarrow[H^+]{H_2O_2} \text{Degradation products} + POM/resin \quad (19)$$

The photodegradation process of RB catalyzed by POM/resin catalyst with H_2O_2 under visible-light irradiation are listed as above equations (16)–(19) (Lei et al., 2005).

It is worth noting that the above mechanism is only appropriately describes the degradation of cationic dyes on POM-embedded anionic resin. Anionic dyes, on the other hand, will undergo another set of mechanisms, attributed to the repulsive forces induced from the same charges. However, the mechanism of such process remains uninvestigated and hence, it is not summarized in current review.

4.2.3. Ternary structure of POM/semiconductor/metal

Ternary structured POM-based nanocomposites reported by Lu et al. (2017) is denoted as such: Ag-TiO_2/$H_3PW_{12}O_{40}$. Its reactivity was evaluated under simulated sunlight with wavelength from 320 to 780 nm, with the aim to mineralize *o*-chlorophenol (*o*-CP). It is claimed that the engineered ternary POM-based nanocomposite is able to functionalize under both irradiations of UV or visible light for the degradation of *o*-CP. The mechanism of photodegradation of *o*-CP utilizing Ag-TiO_2/$H_3PW_{12}O_{40}$ is illustrated in Fig. 9. It is very stunning that the photogenerated electrons could be obtained from TiO_2 under UV light illumination; on the other hand, the photogenerated electrons could also be obtained from Ag under visible light illumination. Thus, the issue of charge recombination is resolved with this engineered ternary structure. Further descriptions are in the next paragraph.

Under the UV-light region, the photons strike on the valence band of TiO_2, followed with the photogenerated electrons excited and jumped to the conduction band of TiO_2. There are two electron trappers, *i.e.* Ag and $H_3PW_{12}O_{40}$, to capture the photogenerated electrons from TiO_2. Schottky junction is constructed between Ag and TiO_2 and then, the electrons on Ag surface could be transferred to adsorbed O_2 to form $\bullet O_2^-$ ion. Similar to Ag, the embedded $H_3PW_{12}O_{40}$ also acts as an electron trapping center by forming $H_3PW_{12}O_{40}^-$ through the consumption of excited-electron. Subsequently, the $H_3PW_{12}O_{40}^-$ ion undergoes a self-regeneration process by ejecting the electron to O_2 adsorbed. Consequently, $H_3PW_{12}O_{40}$ is obtained and accessible for next cycle of electron transportation. The redox cycling continues to ensure the effective transfer of electron, hence prevent the recombination of the photo-generated charges. Finally, the generated $\bullet O_2^-$ active groups from both Ag- and $H_3PW_{12}O_{40}$-assisted transport would be subjected to a series of reaction to form •OH radicals, which helps in the degradation process.

Contrarily, the photo-excitation via visible light irradiation is entirely different from UV light. It is well-known that the band gap of TiO_2 is very wide (3.2 eV), which is not accessible to the excitation of electrons under the visible light irradiation. Ag, however, is able to be activated under this low-energy activator by transforming the hot plasmonic electron to the conduction band of TiO_2. In addition, $H_3PW_{12}O_{40}$, as an excellent electron storage, would also garner the electron from both Ag and conduction band of TiO_2, consecutively interchange between $H_3PW_{12}O_{40}^-$ via the redox cycle as aforementioned. Similar with UV-activated path, continuous supply of O_2 molecules is essentially required to scavenge the electrons generated to alleviate the charges recombination, and hence ensuring the efficiency of the *o*-CP degradation.

To surmise, the superiority of this ternary structure widely extended the light absorption spectrum, covering both UV and visible light region. Both TiO_2 and POM-based composites are only UV responsive. Hence, provisionally encompassing a visible light responsive element or metal, such as Ag, inventively extends the responsive spectrum to visible light region. Similar strategy can be employed in future study for the development of dual-functionalized photocatalyst that works under both UV and visible light region for the degradation of organic pollutants. The prospective materials are desirable to encompassing (Li et al., 2020; Zhang et al., 2019; Zhang et al., 2020): (i) A suitable energy band position, e.g. Bi_2MoO_6, BiOBr, g-C_3N_4, *etc.*, and; (ii) An accelerated photoinduced charge carrier separation and migration efficiency, e.g. Ti_3C_2, carbon dots, carbon quantum dots, *etc.*

5. Conclusion and future prospects

POMs have emerged to be green and eco-friendly photocatalysts that expanded abruptly in various applications. It is touted for their high accessibility, reversible oxidation-reduction to form multivalence species and efficient electron storing ability, which are essentially needed in photocatalysis. Disregarding all the advantages mentioned beforehand, it is undeniably that POMs are still hindered from some unresolved problems, such as large energy bandgap (UV light responsive), low specific surface area, high tendency to pH-induced dissociation, low recoverability, and hence scarce utilization in visible or solar light region.

Several undertakings have been scrupulously scrutinized to resolve the issues aforementioned. Doping of semiconductors, complexation with nonmetal elements, incorporation of organic or inorganic frameworks and other assorted strategies to augment photocatalytic performance of pristine Keggin-based POM photocatalysts. Below are critical factors in correspondence to the insightful strategies in enhancing the practicality application of Keggin-based POM:

1. Extension of light absorption to longer wavelength could be achieved by chemical interlinkage of pertinent extrinsic components of the conceived photocatalytic formulations;
2. Amount of active sites could be boosted with those bulk phasic semiconductors, which contain larger surface areas;
3. The structural stability in alkali-prone solution could be prolonged and sustained by embedding stable scaffoldings or pH impervious substances; and
4. The separation process with low energy consumption could be accomplished by the magnetization synthetic approach compared to centrifugation and vacuum filtration.

Solving these as-mentioned major issues would necessitate the enhanced activity of Keggin-based POM photocatalysts, hence diversifying the application potential and improving the practicality for large-scale implementation. In this review, many incessant endeavors are summarized and discussed. It was initiated with the strategized preparation method, followed by hierarchical enhancement, where the modification of POM photocatalyst and process intensification were endeavored in the aim of improving the practicality. It is believed that the current review work could cast a light on structural tuning of the Keggin-based POM materials, conferring better charge separation, higher specific surface area, wider pH sustainability and higher recoverability in polar environment by scrutinizing closely and thoroughly on others' work. With all the analysis or suggestions assembled, the performance of this material, particularly on photocatalytic activity would be greatly enhanced.

Indeed, researchers have developed a series of heterogeneous Keggin-based POM photocatalysts through different approaches, such as encapsulating of Keggin-based POM within the porous MOF matrix, constructing self-assembly organic-POMs hybrids, immobilizing of POMs on zeolite, SiO_2, porous carbon and g-C_3N_4. However, all these Keggin-based POM photocatalysts were not sufficiently practical for industrial implementation, often due to scarcity of desired properties. A perfect POM photocatalyst should be complimented with large surface area, good electron storage

and conversion that facilitates the photocatalysis activity, at the same time rendered with high structural stability and facile separability for subsequent reactive cycles. Considering these mentioned aspects, heterogenization of POM-based material into MXene could be a potential solution to the problems. MXene is a novel 2D nanomaterials which has a very large interlayer spacing, large surface area and good electron storage. Encapsulating POM into Mxene might induce another novel promising photocatalyst in photodegradation of pollutants without causing environmental issues as both of these materials are greener than others.

In addition to the support-modification, the potential of POM as photocatalyst is still currently under-explored. Current published reports are mainly focuses on the conventional Mo- and W-based POM photocatalyst. Often, the pH-induced dissociation is prevented via inclusion of dopant, support or co-catalyst, which however rarely supported by the fundamental discussion. Most of the time, the stability of the modified POM-based photocatalyst are confirmed via post-reaction photocatalyst characterizations and recyclability test that exhibited similarly as the fresh ones. Therefore, the surface responses and fundamental in maintaining the unchanged structures and performance remains mystery and worth for in-depth investigations. Furthermore, we would like to propose the alternative intrinsic modifications herein, which we believe in their potentials in improving the structural and performance stabilities:

1. Structural substitution of H^+ ion in Keggin-based POM with alkaline or transition metal ions. Conventional POMs, such as $H_3PW_{12}O_{40}$ and $H_3PMo_{12}O_{40}$ are acidic and readily to be hydrolyzed and dissociated in non-acidic environment. Substitution of H^+ ion with alkaline or transition metal ions could effectively balances out the acidity of POM, which potentially improving the pH resilience and dissociation resistance in the non-acidic substrate solution.
2. Formation of mix-valence complexes. Accordingly, the precedent POM photocatalysis reports rarely emphasize on the formation of mix-valence POM complexes via metal-substitution in the skeleton of POM structure. Theoretically, by partially replacing the Mo or W (for $H_3PW_{12}O_{40}$ or $H_3PMo_{12}O_{40}$ respectively) with *d*- and *f*-orbitals metals such as vanadium and bismuth would potentially create more empty orbitals at the conduction band for the enhanced acceptance of photogenerated electrons. Non-metal elements, such as C, S, N, *etc*, can also be taken into consideration for the introduction of mid bandgaps. In addition to extending the responsive light spectrum, it is also vitally important in engineering the bands positions, hence tuning the redox capacity according to the applications.

All in all, we aspire that this review will give the readers overall ideas on the Keggin-based POM photocatalysis by presenting on the strategized preparation methods, hierarchical enhancement *viz.* POM modification and process intensification, and mechanisms supported by the fundamental working principles. With this systematic review manuscript, we also heartily hope that the readers' needs will be well-catered, particularly those that are new to the field of photocatalysis over Keggin-based POM nanocomposites.

Declaration of competing interest

The authors declare that they have no known competing financial interests or personal relationships that could have appeared to influence the work reported in this paper.

Acknowledgments

This research was supported by the Ministry of Higher Education (MOHE) through the Fundamental Research Grant Scheme (FRGS/1/2019/TK02/XMU/03/1) and Xiamen University Malaysia Research Fund (Grant no. XMUMRF/2019-C4/IENG/0019 and XMUMRF/2020-C5/IENG/0029).

References

Ammam, M., 2013. Polyoxometalates: formation, structures, principal properties, main deposition methods and application in sensing. J. Mater. Chem. A 1, 6291.
Antonaraki, S., et al., 2002. Photolytic degradation of all chlorophenols with polyoxometallates and H_2O_2. J. Photochem. Photobiol., A 148, 191–197.
Assran, A.S., et al., 2012. The antimony(III)-bridged heteropolyanion sandwich dimers $[Sb^{III3}(A\text{-}\alpha\text{-}XW_9O_{34})_2]^{11-}$ ($X = Si^{IV}$, Ge^{IV}) and C-shaped double-sandwich $[Sb^{III6}O_2(PW_6O_{26})(A\text{-}\alpha\text{-}PW_9O_{34})_2]^{15-}$. Dalton Trans. 41, 9914.
Bamoharram, F.F., et al., 2013. Cesium salt of sodium 30-tungstopentaphosphate: an effective and green polyoxometalate for synthesis of gold nanoparticles along with decoration of titanium dioxide with gold nanoparticles for bleaching of malachite green. Int. J. Photoenergy 507329.
Björklund, K., Y Li, L., 2017. Adsorption of organic stormwater pollutants onto activated carbon from sewage sludge. J. Environ. Manag. 197, 490–497.
Boussema, F., Gross, Andrew J., Hmida, Fatma, Ayed, Brahim, Majdoub, Hatem, Cosnier, Serge, Maaref, Abderrazak, Holzinger, Michael, et al., 2018. Dawson-type polyoxometalate nanoclusters confined in a carbon nanotube matrix as efficient redox mediators for enzymatic glucose biofuel cell anodes and glucose biosensors. Biosens. Bioelectron. 109, 20–26.
Buru, C.T., et al., 2019. Restricting polyoxometalate movement within metal-organic frameworks to assess the role of residual water in catalytic thioether oxidation using these dynamic composites. Front. Mater. 6, 152.
Castañeda-Juáreza, M., et al., 2019. Synthesis of TiO_2 catalysts doped with Cu, Fe, and Fe/Cu supported on clinoptilolite zeolite by an electrochemical-thermal method for the degradation of diclofenac by heterogeneous photocatalysis. J. Photochem. Photobiol., A 380, 111834.
Cavani, F., 1998. Heteropolycompound-based catalysts: a blend of acid and oxidizing properties. Catal. Today 41, 73–86.
Chen, L., et al., 2019. Polyoxometalates in dye-sensitized solar cells. Chem. Soc. Rev. 48, 260–284.
Cheng, C.K., et al., 2016. Preparation of titania doped argentum photocatalyst and its photoactivity towards palm oil mill effluent degradation. J. Clean. Prod. 112, 1128–1135.
Chiou, C.-H., Juang, R.-S., 2007. Photocatalytic degradation of phenol in aqueous solutions by Pr-doped TiO_2 nanoparticles. J. Hazard Mater. 149, 1–7.
Chiu, Y.-H., et al., 2019. Mechanistic insights into photodegradation of organic dyes using heterostructure photocatalysts. Catalysts 9, 430.
Chowdhary, P., et al., 2017. Green Technologies and Environmental Sustainability. Springer International Publishing.
Deshpande, A.V., Kumar, U., 2002. Effect of method of preparation on photophysical properties of Rh-B impregnated sol–gel hosts. J. Non-Cryst. Solids 306, 149–159.
Dianat, S., et al., 2019. Electrochemical behavior of inorganic–organic hybrid polyoxometalate ($(Cys)_3[PW_{12}O_{40}]$) nanostructure self-assembled monolayer on polycrystalline gold electrode surfaces. New J. Chem. 43, 1388–1397.
Ding, Z., et al., 2012. Preparation of a modified PTFE fibrous photo-fenton catalyst and its optimization towards the degradation of organic dye. Int. J. Photoenergy 2012, 1–8.
Du, M., et al., 2019. Self-assembly and photocatalytic properties of three nanosized polyoxometalates based on the $\{SiNb_3W_9O_{40}\}$ cluster and transition-metal cations. J. Solid State Chem. 277, 618–623.
Fang, X., et al., 2012. A co-crystal of polyoxometalates exhibiting single-molecule magnet behavior: the structural origin of a large magnetic anisotropy. Dalton Trans. 41, 9867.
Farhadi, S., Zaidi, M., 2009. Polyoxometalate–zirconia (POM/ZrO_2) nanocomposite prepared by sol–gel process: a green and recyclable photocatalyst for efficient and selective aerobic oxidation of alcohols into aldehydes and ketones. Appl. Catal. Gen. 354, 119–126.
Feng, J., et al., 2006. Effect of initial solution pH on the degradation of Orange II using clay-based Fe nanocomposites as heterogeneous photo-Fenton catalyst. Water Res. 40, 641–646.
Gao, P., et al., 2016. Co-assembly of polyoxometalates and peptides towards biological applications. Soft Matter 12, 8464–8479.
Ghali, M., et al., 2019. New hybrid polyoxometalate/polymer composites for photodegradation of Eosin dye. J. Polym. Sci. 57, 1538–1549.
Giannakoudakisa, D.A., et al., 2019. Polyoxometalate hybrid catalyst for detection and photodecomposition of mustard gas surrogate vapors. Appl. Surf. Sci. 467–468, 428–438.
Gu, C., Shannon, C., 2007. Investigation of the photocatalytic activity of TiO_2–polyoxometalate systems for the oxidation of methanol. J. Mol. Catal. A Chem. 262, 185–189.
Guo, Y., Hu, C., 2007. Heterogeneous photocatalysis by solid polyoxometalates. J. Mol. Catal. A Chem. 262, 136–148.

Guo, Y., et al., 2000. Microporous polyoxometalates POMs/SiO_2: Synthesis and photocatalytic degradation of aqueous organocholorine pesticides. Chem. Mater. 12, 3501–3508.
Heravi, M.M., et al., 2013. Heteropoly acids-catalyzed organic reactions in water: doubly green reactions. Green Chem. Lett. Rev. 6, 282–300.
Hill, C.L., 2007. Progress and challenges in polyoxometalate-based catalysis and catalytic materials chemistry. J. Mol. Catal. A Chem. 262, 2–6.
Hir, Z.A.M., et al., 2017. Immobilization of TiO_2 into polyethersulfone matrix as hybrid film photocatalyst for effective degradation of methyl orange dye. Mater. Sci. Semicond. Process. 57, 157–165.
Holclajtner-Antunović, I., et al., 2019. Ethanol dehydration over Keggin type tungstophosphoric acid and its potassium salts supported on carbon. React. Kinet. Mech. Catal. 128, 121–137.
Hu, B., et al., 2012. Inorganic–organic hybrid compounds based on novel lanthanide-antimony oxohalide nanoclusters. Dalton Trans. 33, 9879.
Hu, J., et al., 2019. In-situ Fe-doped g-C_3N_4 heterogeneous catalyst via photocatalysis-Fenton reaction with enriched photocatalytic performance for removal of complex wastewater. Appl. Catal. B Environ. 245, 130–142.
Hu, M., Xu, Y., 2004. Photocatalytic degradation of textile dye X3B by heteropolyoxometalate acids. Chemosphere 54, 431–434.
Huang, X., Liu, X., 2020. Morphology control of highly efficient visible-light driven carbon-doped POM photocatalysts. Appl. Surf. Sci. 505, 144527.
Huang, Yongkui, Yang, Zhiyuan, Yang, Shuijin, Xu, Yulin, et al., 2017. Photodegradation of dye pollutants catalyzed by $H_3PW_{12}O_{40}/SiO_2$ treated with H_2O_2 under stimulated solar light irradiation. J. Adv. Nanomater. 2, 146–152.
Jamshidi, A., et al., 2020. A new Keggin-based organic-inorganic nanohybrid in the role of a dual-purpose catalyst. J. Chem. Sci. 132, 37.
Jin, Z., et al., 2013. Synthesis, characterization and photocatalytic application of $H_3PW_{12}O_{40}/BiVO_4$ composite photocatalyst. Sci. China Chem. 56, 1285–1292.
Karimian, D., et al., 2017. Dual functional hybrid-polyoxometalate as a new approach formultidrug delivery. Microporous Mesoporous Mater. 247, 23–30.
Kato, C.N., et al., 2012. Diplatinum(ii)-coordinated polyoxotungstate: synthesis, molecular structure, and photocatalytic performance for hydrogen evolution from water under visible-light irradiation. Dalton Trans. 41, 10021.
Kazemi, H.S.A.T.S., 2017. Investigation of photocatalytic performance of Keggin type heteropolyacid in degradation of methylene blue. Chem. Methodol. 1, 145–158.
Kazemi, S., et al., 2017. Developments of modified magnetic nanoparticle-supported heteropolyacid photocatalytic performances in methylene blue scavenger. J. Chin. Chem. Soc. 65, 1218–1228.
Kazemi, S., et al., 2018. Developments of modified magnetic nanoparticle-supported heteropolyacid photocatalytic performances in methylene blue scavenger. J. Chin. Chem. Soc. 65, 1218–1228.
Keita, B., et al., 2006. Reactions of V-substituted polyoxometalates with L-cysteine. J. Cluster Sci. 17, 221–233.
Kozhevnikov, I.V., 1998. Catalysis by heteropoly acids and multicomponent polyoxometalates in liquid-phase reactions. Chem. Rev. 98, 171–198.
Kumar, D., Landry, C., 2007. Immobilization of a Mo , V-polyoxometalate on cationically modified mesoporous silica : synthesis and characterization studies. Microporous Mesoporous Mater. 98, 309–316.
Lan, Q., et al., 2016. Highly dispersed polyoxometalate-doped porous Co_3O_4 water oxidation photocatalysts derived from POM@MOF crystalline materials. Chem. Eur J. 22, 1–9.
Lei, P., et al., 2005. Degradation of dye pollutants by immobilized polyoxometalate with H_2O_2 under visible-light irradiation. Environ. Sci. Technol. 39, 8466–8474.
Li, B., et al., 2020. Unravelling the interfacial charge migration pathway at atomic level in 2D/2D interfacial Schottky heterojunction for visible-light-driven molecular oxygen activation. Appl. Catal. B Environ. 266, 118650.
Li, F., et al., 2015. Removal of rhodamine B and Cr(VI) from aqueous solutions by a polyoxometalate adsorbent. Chem. Eng. Res. Des. 100, 192–202.
Li, F., et al., 2012. Cation induced structural transformation and mass spectrometric observation of the missing dodecavanadomanganate(IV). Dalton Trans. 41, 9859.
Li, G., et al., 2019a. Solvent-free method to encapsulate polyoxometalate into metal-organic frameworks as efficient and recyclable photocatalyst for harmful sulfamethazine degrading in water. Appl. Catal. B Environ. 245, 753–759.
Li, H., et al., 2014. Self-assembly of hierarchical nanostructures from dopamine and polyoxometalate for oral drug delivery. Chem. Eur J. 20, 499–504.
Li, H., et al., 2018. Charge-regulated sequential adsorption of anionic catalysts and cationic photosensitizers into metal-organic frameworks enhances photocatalytic proton reduction. Appl. Catal. B Environ. 224, 46–52.
Li, L., et al., 2019b. Optimization of degradation kinetics towards O-CP in $H_3PW_{12}O_{40}/TiO_2$ photoelectrocatalytic system. Sustainability 11, 3551.
Li, T., et al., 2017. Polyoxometalate (POM)-layered double hydroxides (LDH) composite materials: design and catalytic applications. Catalysts 7, 260.
Li, X.-X., et al., 2019c. Recent advances in POM-organic frameworks and POM-organic polyhedra. Coord. Chem. Rev. 397, 220–240.
Liang, C., et al., 2017. Influence of precursor pH on the structure and photo-Fenton performance of Fe/hydrochar. RSC Adv. 7, 35257–35264.
Liu, G., et al., 2018a. Z-scheme Ag_3PO_4/POM/GO heterojunction with enhanced photocatalytic performance for degradation and water splitting. Dalton Trans. 47, 6225.
Liu, M., et al., 2018b. A robust polyoxometalate-templated four-fold interpenetrating metal-organic framework showing efficient organic dye photodegradation in various pH aqueous solutions. Dalton Trans. 47, 5245.
Liu, P., et al., 2011. A general strategy to fabricate simple polyoxometalate nanostructures: electrochemistry-assisted laser ablation in liquid. ACS Nano 5, 4748–4755.
Lu, N., et al., 2017. Design of plasmonic Ag-$TiO_2/H_3PW_{12}O_{40}$ composite film with enhanced sunlight photocatalytic activity towards o-chlorophenol degradation. Sci. Rep. 7, 17298.
Lu, N., et al., 2012. Design of polyoxometalate-titania composite film ($H_3PW_{12}O_{40}/TiO_2$) for the degradation of an aqueous dye Rhodamine B under the simulated sunlight irradiation. J. Hazard Mater. 199–200, 1–8.
Luo, Y.-H., et al., 2016. Assembly of a high stable POM-based Cu(I) coordination polymer with visible-light-driven photocatalytic properties. Inorg. Chem. Commun. 72, 13–16.
Luo, Y., et al., 2018. Direct detection of the photoinduced charge-separated state in a Ru(II) bis(terpyridine)-polyoxometalate molecular dyad. Chem. Commun. 54, 2970.
Lv, H., et al., 2012. Polyoxometalate water oxidation catalysts and the production of green fuel. Chem. Soc. Rev. 41, 7572–7589.
M, M., M, J., 2017. Synthesis, characterization and investigation of photocatalytic activity of $H_3PMO_{12}O_{40}/TiO_2$/HY nanocomposite for degradation of methyl orange in aqueous media. Modern Chem. Appl. 5, 1000205.
Ma, Y., et al., 2018. Polyoxometalate-based metal-organic frameworks for selective oxidation of aryl alkenes to aldehydes. Inorg. Chem. 57, 4109–4116.
Maguerès, P.L., et al., 2000. Novel charge-transfer materials via cocrystallization of planar aromatic donors and spherical polyoxometalate acceptors. J. Am. Chem. Soc. 122, 10073–10082.
Mahmoodi, N.M., et al., 2016. Immobilized polyoxometalate onto the modified magnetic nanoparticle as a photocatalyst for dye degradation. Mater. Res. Bull. 84, 422–428.
Meng, P., et al., 2019. In-situ solid phase thermal transformation of self-assembled melamine phosphotungstates produce efficient visible light photocatalysts. J. Colloid Interface Sci. 551.
Mercier, D., et al., 2015. Polyoxometalate nanostructured gold surfaces for sensitive biosensing of benzo[a]pyrene. Sensor. Actuator. B Chem. 209, 770–774.
Mizuno, N., et al., 2005. Epoxidation of olefins with hydrogen peroxide catalyzed by polyoxometalates. Coord. Chem. Rev. 249, 1944–1956.
Nandi, B.K., et al., 2009. Adsorption characteristics of brilliant green dye on kaolin. J. Hazard Mater. 161, 387–395.
Ng, K.H., Cheng, C.K., 2015. A novel photomineralization of POME over UV-responsive TiO_2 photocatalyst: kinetics of POME degradation and gaseous product formations. RSC Adv. 5, 53100–53110.
Ng, K.H., Cheng, C.K., 2016. Photo-polishing of POME into CH4-lean biogas over the UV-responsive ZnO photocatalyst. Chem. Eng. J. 300, 127–138.
Ng, K.H., Cheng, C.K., 2017. Photocatalytic degradation of palm oil mill effluent over ultraviolet-responsive titania: successive assessments of significance factors and process optimization. J. Clean. Prod. 142, 2073–2083.
Ng, K.H., et al., 2016a. Optimization of photocatalytic degradation of palm oil mill effluent in UV/ZnO system based on response surface methodology. J. Environ. Manag. 184, 487–493.
Ng, K.H., et al., 2017. Restoration of liquid effluent from oil palm agroindustry in Malaysia using UV/TiO_2 and UV/ZnO photocatalytic systems: a comparative study. J. Environ. Manag. 196, 674–680.
Ng, K.H., et al., 2016b. Photocatalytic degradation of recalcitrant POME waste by using silver doped titania: photokinetics and scavenging studies. Chem. Eng. J. 286, 282–290.
Ng, K.H., et al., 2019. TiO_2 and ZnO photocatalytic treatment of palm oil mill effluent (POME) and feasibility of renewable energy generation: a short review. J. Clean. Prod. 233, 209–225.
Nicholson, B.K., et al., 2012. Isopolyoxometalates derived from arylstibonic acids with "reverse-Keggin ion" structures based on $[M(RSb)_{12}O_{28}]$ cores, M = Co(ii) or Zn(ii). Dalton Trans. 41, 9964.
Nikoonahad, A., et al., 2018. An overview report on the application of heteropoly acids on supporting materials in the photocatalytic degradation of organic pollutants from aqueous solutions. PeerJ 6 (e5501), 1–20.
Niu, P., et al., 2018. Fabrication of bifunctional TiO_2/POM microspheres using a layer-by-layer method and photocatalytic activity for methyl orange degradation. J. Nanomater. 1–8.
Nur, H., et al., 2014. Synthesis of titania with different shapes. *2014* International Renewable and Sustainable Energy Conference (IRSEC) 531–535. https://doi.org/10.1109/IRSEC.2014.7059840.
Ogo, S., et al., 2012. Hydrothermal and solid-state transformation of ruthenium-supported Keggin-type heteropolytungstates $[XW_{11}O_{39}\{Ru(ii)(benzene)(H_2O)\}]n-$ (X = P (n = 5), Si (n = 6), Ge (n = 6)) to ruthenium-substituted Keggin-type heteropolytungstates. Dalton Trans. 41, 9901.
Oliveira, A.d.N.d., et al., 2019. Bentonites modified with phosphomolybdic heteropolyacid (HPMo) for biowaste to biofuel production. Materials 12, 1431.
Omwoma, S., et al., 2014. Environmentally-benign polyoxometalate materials. Coord. Chem. Rev. 286, 17–29.
Qian, X., et al., 2012. Synthesis and electrochemical properties of substituted heteropoly acid with Dawson structure $H_7[In(H_2O)P_2W_{17}O_{61}]\cdot 23H_2O$. Dalton Trans. 41, 9897.
Qiu, W., et al., 2007. Study on a novel POM-based magnetic photocatalyst: photocatalytic degradation and magnetic separation. Chem. Eng. J. 125, 165–176.
Rafiee, E., et al., 2020. A new polyoxometalate-TiO_2 nanocomposite for efficient visible photodegradation of dye from wastewater, liquorice and yeast extract: photoelectrochemical, electrochemical, and physical investigations. J. Photochem. Photobiol., A 386, 112145.

Ramalingam, M., et al., 2019. N-doped carbon wrapped polyoxometalate derived from POM-IL hybrid: a heterogeneous catalyst for the synthesis of coumarin derivatives under solvent-free conditions. Eur. J. Inorg. Chem. 1904–1910.
Razali, R., et al., 2014. Some aspects of particuology in heterogeneous catalysts. J. Teknol. 69, 2180–3722.
Rengaraj, S., et al., 2007. Preparation, characterization and application of Nd–TiO_2 photocatalyst for the reduction of Cr(VI) under UV light illumination. Appl. Catal. B Environ. 77, 157–162.
Rohani, N., et al., 2017. Gold nanoparticles Wells-Dawson heteropolyacid nanocomposite film as an effective nanocatalyst in photocatalytic removal of azo dyes from wastewaters. J. Nanostructure Chem. 7, 171–178.
Sagban, T., 2014. Organic micro pollutants in wastewater sludge. J. Pollut. Effects Control 2, 1000e1108.
Salavati, H., et al., 2018. Synthesis and characterization of nanocomposite-based heteropolyacid, and its catalytic, photocatalytic and electrochemical performances. Int. J. Electrochem. Sci. 13, 2887–2910.
Sampurnam, S., et al., 2018. Synthesis, characterization and heterogeneous photocatalytic activity of $H_3PW_{12}O_{40}/TiO_2$/Ag composites. Mater. Today: Proceedings 5, 8808–8811.
Shahrnoya, A.A., et al., 2018. Sonochemical synthesis of polyoxometalate based of ionic crystal nanostructure: a photocatalyst for degradation of 2,4-dichlorophenol. Ultrason. Sonochem. 40, 174–183.
Shi, H., et al., 2012. Enhancement of photocatalytic activity of nano-scale TiO_2 particles co-doped by rare earth elements and heteropolyacids. J. Colloid Interface Sci. 380, 121–127.
Shi, H., et al., 2019. Pr/POMs/TiO_2 composite nanofibers with an enhanced visible-light photocatalytic performance for environmental remediation. Dalton Trans. 48, 13353.
Shi, Y.-L., et al., 2006. Synthesis and characterization of a POM-based nanocomposite as a novel magnetic photocatalyst. J. Phys. Chem. Solid. 67, 2409–2418.
Sokolov, M.N., et al., 2012. Organometallic derivatives of Rh- and Ir-substituted polyoxotungstates with Keggin structure: reactivity screening by electrospray ionization mass-spectrometry. Dalton Trans. 41, 9889.
Song, Y., et al., 2020. Effect of mixed Mo/W polyoxometalate modification on photoelectrocatalytic activity of CdS nanocrystals for arsenic(III) oxidation. J. Phys. Chem. Solid. 141, 109395.
Streb, C., et al., 2019. Polyoxometalates in photocatalysis. Phys. Sci. Rev. (20170177), 1–10.
Stuckart, M., Monakhov, K.Y., 2018. Polyoxometalate encapsulation into metal–organic frameworks: the way towards functional nanomaterials for water splitting. J. Mater. Chem. A 6, 17849.
Suzuki, K., et al., 2018. Polyoxometalate photocatalysis for liquid-phase selective organic functional group transformations. ACS Catal. 8, 10809–10825.
Taghavi, M., et al., 2018. Application of a Keggin-type heteropoly acid on supporting nanoparticles in photocatalytic degradation of organic pollutants in aqueous solutions. J. Clean. Prod. 197, 1447–1453.
Taghizadeh, M., et al., 2019. Polyoxometalate as an effective catalyst for the oxidative desulfurization of liquid fuels: a critical review. Rev. Chem. Eng. 1–29.
Tang, Q., et al., 2020. Polyoxometalates/TiO_2 photocatalysts with engineered facets for enhanced degradation of bisphenol A through persulfate activation. Appl. Catal. B Environ. 268, 118394.
Tang, Z., et al., 2000. Preparation, structures, and electrochemistry of a new polyoxometalate-based organic/inorganic film on carbon surfaces. Langmuir 16, 5806–5813.
Tarmizi, E.Z.M., et al., 2018. Preparation and physical properties of polypyrrole/zeolite composites. Results Phys 11, 793–800.
Tayebee, R., et al., 2019. $H_3PW_{12}O_{40}$/SBA-15 for the solventless synthesis of 3-substituted Indoles. Catalysts 9, 409.
Tiejun, C., et al., 2009. Photocatalytic performance of TiO_2 catalysts modified by $H_3PW_{12}O_{40}$, ZrO_2 and CeO_2. J. Environ. Sci. 21, 997–1004.
Tong, X., et al., 2012. Pentadecatungstotrivanadodiphosphoric heteropoly acid with Dawson structure: synthesis, conductivity and conductive mechanism. Dalton Trans. 41 (33), 9893.
Wang, J., et al., 2019. Multivalent supramolecular self-assembly between β-cyclodextrin derivatives and polyoxometalate for photodegradation of dyes and antibiotics. ACS Appl. Bio Mater. 2, 5898–5904.
Wang, J., et al., 2012. Polyoxometalates as peroxidase mimetics and their applications in H_2O_2 and glucose detection. Biosens. Bioelectron. 36, 18–21.
Wang, Q., et al., 2017. Preparation of visible-light-driven BiOBr composites with heteropolyacids ($H_3PW_{12}O_{40}$) encapsulated by a zeolite for the photodegradation of methyl orange. New J. Chem. 41, 4322–4328.
Wang, S.-S., Yang, G.-Y., 2015. Recent advances in polyoxometalate-catalyzed reactions. Chem. Rev. 115, 4893–4962.
Wang, Y., et al., 2013. Influence of inorganic anions and organic additives on photocatalytic degradation of methyl orange with supported polyoxometalates as photocatalyst. J. Rare Earths 31, 360–365.
Wu, H., et al., 2020. Sulfur-doping polyoxometallate-metal-organic intercalation compound with PPy coating as highly efficient photocatalyst for visible light degradation. Polyhedron 179, 114350.
Wu, X., et al., 2013. Synthesis of high visible light active carbon doped TiO_2 photocatalyst by a facile calcination assisted solvothermal method. Appl. Catal. B Environ. 142–143, 450–457.
Xu, Y., et al., 2016. Rational design of semiconductor-based photocatalysts for advanced photocatalytic hydrogen production: the case of cadmium chalcogenides. Inorg. Chem. Front. 3, 591–615.
Yahya, F., et al., 2019. Synthesis and characterisation of mesoporous hybrid silica-polyoxometalate aerogels for photocatalytic degradation of rhodamine B and methylene blue. Int. J. Environ. Anal. Chem. 99, 1375–1396.
Yan, G., et al., 2017. Tuning of the photocatalytic performance of g-C_3N_4 by polyoxometalates under visible light. Dalton Trans. 46, 16019–16024.
Yang, L.-b., et al., 2009. Advances in self-assembled ultrathin polyoxomolybdates multilayers. Front. Mater. Sci. 3, 1–8.
Yang, S., et al., 2012. Photocatalytic degradation of rhodamine B with $H_3PW_{12}O_{40}$/SiO_2 sensitized by H_2O_2. Int. J. Photoenergy (2012), 1–6.
Yang, Y., et al., 2005. Efficient degradation of dye pollutants on nanoporous polyoxotungstate-anatase composite under visible-light irradiation. J. Mol. Catal. Chem. 225, 203–212.
Yoon, M., et al., 2001. Heteropoly acid-incorporated TiO_2 colloids as novel photocatalytic systems resembling the photosynthetic reaction center. J. Phys. Chem. B 105, 2539–2545.
Yu, J., et al., 2019. Magnetically separable TiO_2/FeOx/POM accelerating the photocatalytic removal of the emerging endocrine disruptor: 2,4-dichlorophenol. Appl. Catal. B Environ. 254, 66–75.
Yue, B., et al., 2002. Photocatalytic degradation of aqueous 4-chlorophenol by silica-immobilized polyoxometalates. Environ. Sci. Technol. 36, 1325–1329.
Zhai, Q., et al., 2016. A novel iron-containing polyoxometalate heterogeneous photocatalyst for efficient 4-chlorophennol degradation by H_2O_2 at neutral pH. Appl. Surf. Sci. 377, 17–22.
Zhang, D., et al., 2020a. Preparation of vanadium-substituted polyoxometalate doped carbon nitride hybrid materials POM/g-C_3N_4 and their photocatalytic oxidation performance. Mater. Lett. 262, 126954.
Zhang, M., et al., 2019. Rational design 2D/2D BiOBr/CDs/g-C_3N_4 Z-scheme heterojunction photocatalyst with carbon dots as solid-state electron mediators for enhanced visible and NIR photocatalytic activity: kinetics, intermediates, and mechanism insight. J. Catal. 369, 469–481.
Zhang, M., et al., 2020b. Unravelling the role of dual quantum dots cocatalyst in 0D/2D heterojunction photocatalyst for promoting photocatalytic organic pollutant degradation. Chem. Eng. J. 396, 125343.
Zhang, M., et al., 2017. Magnetic POM-based mesoporous silica for fast oxidation of aromatic sulfur compounds. Fuel 209, 545–551.
Zhao, G., et al., 2018a. Constructing and controlling of highly dispersed metallic sites for catalysis. Nano Today 19, 108–125.
Zhao, K., et al., 2013. Design of $H_3PW_{12}O_{40}/TiO_2$ nano-photocatalyst for efficient photocatalysis under simulated sunlight irradiation. Appl. Surf. Sci. 285, 616–624.
Zhao, S.-N., et al., 2018b. Metal organic frameworks based materials for heterogeneous photocatalysis. Molecules 23, 2947.
Zhao, X., et al., 2018c. Polyoxometalate-based metal–organic frameworks as visible-light-induced photocatalysts. Inorg. Chem. 57, 5030–5037.
Zhao, Y., et al., 2020. Self-assembled gels of Fe-chitosan/montmorillonite nanosheets: dye degradation by the synergistic effect of adsorption and photo-Fenton reaction. Chem. Eng. J. 379, 122322.
Zheng, Y.-Y., et al., 2012. Assembly of an undeca-nuclear nickel substituted POM through polycarboxylate ligand. Dalton Trans. 41, 9871.
Zhou, C., et al., 2013. A sensor of a polyoxometalate and Au–Pd alloy for simultaneously detection of dopamine and ascorbic acid. Electrochim. Acta 113, 454–463.
Zhou, X., et al., 2019. Combination of polyoxotantalate and metal sulfide: a new-type noble-metal-free binary photocatalyst $Na_8Ta_6O_{19}/Cd_{0.7}Zn_{0.3}S$ for highly efficient visible-light-driven H_2 evolution. Appl. Catal. B Environ. 248, 423–429.
Zi, S.C., et al., 2016. New method to synthesize mesoporous titania by photodegradation of surfactant template. Solid State Sci. 52, 83–91.